Tumor-derived prostaglandin E2 promotes p50 NF-κB-dependent differentiation of monocytic MDSC

Chiara Porta[1,9], Francesca M. Consonni[2], Sara Morlacchi[2], Sabina Sangaletti[3], Augusto Bleve[1], Maria G. Totaro[2], Paola Larghi[2], Monica Rimoldi[2], Claudio Tripodo[4], Laura Strauss[1], Stefania Banfi[2], Mariangela Storto[2], Tiziana Pressiani[2], Lorenza Rimassa[2], Silvia Tartari[2], Alessandro Ippolito[1], Andrea Doni[2], Giulia Soldà[2,5], Stefano Duga[2,5], Viviana Piccolo[2], Renato Ostuni[6], Gioacchino Natoli[2,5], Vincenzo Bronte[7], Fiorella Balzac[8], Emilia Turco[8], Emilio Hirsch[8], Mario P. Colombo[3] and Antonio Sica[1,2]

[1]Department of Pharmaceutical Sciences, Università del Piemonte Orientale "Amedeo Avogadro", via Bovio 6, 28100 Novara, Italy.

[2] Humanitas Clinical and Research Center, Via Manzoni 56, 20089 Rozzano, Milan, Italy.

[3]Fondazione IRCCS Istituto Nazionale dei Tumori, Milan, Italy

[4]Human Pathology Section, Department of Health Sciences, University of Palermo, Italy

[5]Department of Biomedical Sciences, Humanitas University, via Rita Levi Montalcini 4, Pieve Emanuele, Milan, Italy

[6]San Raffaele Telethon Institute for Gene Therapy, 20132, Milan, Italy.

[7]Department of Medicine, Verona University Hospital, 37134 Verona, Italy

[8]Department of Molecular Biotechnology and Health Sciences, Molecular Biotechnology Center, University of Torino, Via Nizza 52, 10126 Torino, Italy

[9] Center for Translational Research on Autoimmune & Allergic Diseases (CAAD) Cso Trieste 15/A, 28100 Novara, Italy

The first two authors contributed equally to this study

Running title: p50 NF-κB promotes M-MDSC suppressive functions

Corresponding author: Antonio Sica**,** Humanitas Clinical and Cancer Center, 20089 Rozzano, Milan and University of Piemonte Orientale, A. Avogadro, Novara, Italy. Phone: +39.02.8224.5111; Fax:+39.02.8224.5101; Email: antonio.sica@uniupo.it; antonio.sica@humanitasresearch.it (Orcid : 0000-0002-8342-7442)

ABSTRACT

Myeloid-derived suppressor cells (MDSC) include immature monocytic (M-MDSC) and granulocytic (PMN-MDSC) cells that share the ability to suppress adaptive immunity and hinder the effectiveness of anti-cancer treatments. Of note, in response to interferon-γ (IFNγ) M-MDSC release the tumor-promoting and immunosuppressive molecule nitric oxide (NO), whereas macrophages largely express anti-tumor properties. Investigating these opposing activities, we found that tumor-derived prostaglandin E2 (PGE2) induces nuclear accumulation of p50 NF-κB in M-MDSC, diverting their response to IFNγ towards NO-mediated immunosuppression and reducing TNFα expression. At the genome level, p50 NF-κB promoted binding of STAT1 to regulatory

regions of selected IFNγ-dependent genes, including inducible nitric oxide synthase (Nos2). In agreement, ablation of p50 as well as pharmacological inhibition of either the PGE2 receptor EP2 or NO production reprogrammed M-MDSC towards a $NOS2^{low}/TNF\alpha^{high}$ phenotype, restoring the *in vivo* antitumor activity of IFNγ. Our results indicate that inhibition of the PGE2/p50/NO axis prevents MDSC suppressive functions and restores the efficacy of anticancer immunotherapy.

SIGNIFICANCE

Tumor-derived PGE2-mediated induction of nuclear p50 NF-κB epigenetically reprograms the response of monocytic cells to IFNγ towards an immunosuppressive phenotype, thus retrieving the anticancer properties of IFNγ.

INTRODUCTION

Microenvironmental signals are sensed by myeloid cells through cytokine and/or innate immune receptors, whose differential engagement leads different polarized programs (1,2). This functional plasticity is exemplified in the M1 *vs* M2 extremes of macrophage polarization (1-3) and has major impacts in the orchestration of cancer-related inflammation, immunosuppression (4-6) and clinical responses (2,7). Of note, a time-dependent M1 to M2 transcriptional reprogramming of myeloid cells was reported in response to prolonged exposure to Toll-like receptors (TLR) ligands (e.g. lipopolisaccharide) (i.e. LPS tolerance) (8,9), which requires the nuclear accumulation of p50 NF-κB and results in altered responsiveness to

polarizing cytokines, such as IFNγ and IL-4 (9). Cancer fuels myeloid cells heterogeneity also by sustaining altered myelopoiesis (10-13) that supports resistance to anticancer immunotherapy (14). Of relevance, divergent outcomes have been reported in response to immunotherapy, either with cytokines (15-17) or checkpoint inhibitors (18,19). In particular, IFNγ, originally termed “macrophage activating factor” (20), was paradoxically shown to be equally necessary for melanoma development and rejection (21). Indeed, IFNγ has pleiotropic and contrasting effects in the tumor microenvironment. On one hand it exerts anti-angiogenic activities, suppression of pro-tumorigenic properties, enhancement of tumoricidal activity of macrophages and of processing and presentation of tumor antigens to T lymphocytes (17,22). On the other hand, IFNγ promotes immunosuppressive functions in myeloid cells (13) inducing expression of the immunosuppressive enzymes indoleamine 2,3 dioxygenase (*Ido*) and inducible nitric oxide synthase (*Nos2*), involved in the catabolism of L-tryptophan (23) and L-arginine (12), as well as the ligand programmed-death receptor-ligand 1 (PD-L1, B7-H1) (24), whose interaction with the coinhibitory receptor Programmed Death-1 (PD-1) can be blocked to restore antitumor immunity (25). Mixed responses to IFNγ were also reported in different human malignancies (16,17,26). We have previously reported that accumulation of nuclear p50 NF-κB plays an essential role in the M2 orientation of tumor-associated macrophages (TAM) (9,10), which share common myeloid precursors and a similar M2-like gene signature with M-MDSC (10). Here, we investigated how tumor-derived signals affect transcriptional activities and myeloid cell functions in response to immune

stimulatory cytokines and the impact of these events on cytokine-mediated cancer immunotherapy.

MATERIALS and METHODS

Mice and ethics statement. The study was designed in compliance with: Italian Governing Law (Legislative Decree 116 of Jan. 27, 1992); EU directives and guidelines (EEC Council Directive 86/609, OJ L 358, 12/12/1986); Legislative Decree September 19, 1994, n. 626 (89/391/CEE, 89/654/CEE, 89/655/CEE, 89/656/CEE, 90/269/CEE, 90/270/CEE, 90/394/CEE, 90/679/CEE); the NIH Guide for the Care and Use of Laboratory Animals (1996 edition). All experiments involving animals described in this study were approved by the Ministry of Health (authorization numbers 160/2012-B and 25/2018-PR). The study was approved by the scientific board of Humanitas Clinical and Research Center. Mice have been monitored daily and euthanized when displaying excessive discomfort. p50 NF-κB deficient mice on the C57BL/6J background were available in the laboratory(27). The NFKB1flox/flox ($p50^{flox}$) mice was recently generated (28). $p50^{flox}$ mice were crossed with B6.Cg-Tg(Tek-Cre)1Ywa mice (Jackson Laboratories, Bar Harbor, Maine, USA) to generate $p50^{flox}$; Tie2Cre mice ($p50^{Tie2}$ mice). OT-I mice were obtained from Jackson Laboratories (Bar Harbor, Maine, USA).

Tumor models. 8 weeks old mice were injected intramuscularly in the left leg with 10^5 cells of murine fibrosarcoma (MN/MCA1) or subcutaneously with $5x10^5$ cells of murine melanoma (B16). Tumor growth was monitored 3 times a week with a caliper. Bone marrow transfer and schedule of treatments are described in the supplementary Material & Methods

MDSC's purification. MDSC's purification from the spleens of tumor-bearing mice has been performed by magnetic separation (MACS Miltenyi) (11), as described in the supplementary Materials & Methods.

Cell culture and reagents for mouse studies. Bone marrow MDSC (BM-MDSC) were derived from bone marrows (BM) cells isolated from C57BL/6 mice as previously described (29) and reported in the supplementary Materials & Methods. Peritoneal Exudate Macrophages (PEC) were obtained as previously described (10). Preparation of MN/MCA1 tumor supernatant (TSN) and reagents used for mouse studies are described in the supplementary Materials & Methods.

Cell culture and reagents for human studies Human monocytes were isolated from peripheral blood as previously described (9) and cultured in RPMI-1640 containing 10% FBS, 2 mmol/L glutamine, 100 units/mL penicillin-streptomycin. Culture of human pancreatic carcinoma cell line PANC1 and preparation of tumor-conditioned supernatant (TSN) are described in the supplementary Materials & Methods.

The concentration for the different treatments were as follows: PANC1 supernatant (30%), human IFNγ (Peprotech) 20ng/ml, PGE2 receptor (EP2/EP1) antagonist AH6809 (Tocris) 10^{-5} mol/L.

Nitrite production. $2*10^5$ cells were plated and stimulated with IFNγ (Peprotech 200U/ml) for indicated time points. Nitric oxide production was evaluated in culture supernatant using the Griess Reagent System (Promega) as described in supplementary Material & Methods.

Suppression assay M-MDSCs ($CD11b^+Ly6C^+Ly6G^-$ cells) and PMN-MDSCs

(CD11b^{+}Ly6C$^{low/-}$Ly6G^{+} cells) were isolated from spleen and tumor of WT and p50$^{-/-}$ MN-MCA1 tumor-bearing mice. 2x10^{5} splenocytes from naive C57Bl6 mice were labelled with 1μM CFSE and then co-cultured with 1x10^{5}, 5x10^{4} or 2.5x10^{4} WT M-MDSCs, in the presence of anti-CD3 (3 μg/ml, 2C11, Biolegend) and anti-CD28 (2μg/ml, 37.5, BD). Similarly, M- and PMN-MDSC from WT and p50-/- mice were stimulated with IFNγ (200U/ml) for 3 days and then co-cultured with activated CSFE-labeled splenocytes. After 3 days of co-colture, cells were stained and CFSE signal of gated lymphocytes was used to analyze cell proliferation. For antigen-specific suppression assay Mixed-lymphocyte reaction (MLR) was performed as previously reported (11) M-MDSC isolated from the spleen of tumor bearing mice were then stimulated with IFNγ (200U/ml), in the presence or absence of 500μM of L-NG-monomethylarginine (L-NMMA, Calbiochem). At day 3, 50 μl of supernatant were tested for NO production (as control) and 2x10^{5} splenocytes from OT-I mice were added for additional 72h in the presence of 250 μg/ml of ovalbumin peptide (OVA257–264) (Sigma). [3H] thymidine was added for the last 16 hours of culture and its incorporation was analyzed by MicroBeta plate counter (Perkin Elmer). As controls OT-1 splenocytes alone were pulsed with OVA peptide (250 μg/mL) or kept in culture media. All conditions were evaluated in triplicates.

Isolation of MDSCs from colorectal cancer (CRC) patients. The study was conducted in accordance with recognized ethical guidelines (Declaration of Helsinki) was approved by the Institute Ethical Committee, and written informed consent was obtained from 20 patients. 20 ml of peripheral blood were collected from healthy donors and T2 or T3 CRC patients. CRC patients

did not receive radiation or chemotherapy before sample collection. Blood was stratified on Ficoll gradient to separate peripheral blood mononuclear cells (PBMC). All blood samples were analysed within 3 hr after collection by FACS-analysis. Briefly, $1*10^6$ cells were re-suspended in HBSS (Hank's balanced salt solution, Lonza) supplemented with 0.5% BSA (Sigma). Staining was performed at 4°C for 30 minutes, with a cocktail of mABs to HLA-DR-Pacific Blue (clone L243); CD14-PE, -APC, -FITC (clone M5E2); CD33-PerCp-Cy5.5 (clone WM53); iNOS/NOS Type II-FITC (Clone 6/iNOS/NOS Type II), from BD Bioscence or BioLegend. Further we used unconjugated rabbit monoclonal anti human EP2R (clone EPR8030(B); Abcam) followed by incubation with secondary goat anti rabbit Alexa Fluor® 488 conjugated antibody (Life Technologies). For intra-cellular staining, Foxp3/Transcription Factor Staining Buffer Set (eBioscence) were used according to the manufacturer's instruction. Cells were analyzed using the BD FACSCanto™ II or BD LSRFortessa™ and BD FACSDiva and FlowJo (9.3.2) software. When needed, cells were stained, sorted using a BD FACSAria™ III cell sorter and subsequently analyzed by confocal microscopy.

Bone marrow (BM) colony formation. BM cells were isolated from the tibias and femurs of WT or $p50^{-/-}$ mice and the colony formation capacity was measured by detection and quantification using MethoCultTM GF M3434, that supports optimal growth of granulocyte-macrophage progenitors (CFU-GM, CFU-M, CFU-G), of erythroid progenitors (BFU-E) and and multi-potential granulocyte, erythroid, macrophage, megakaryocyte progenitors (CFU-GEMM). 12 days after seeded, colonies were counted independently by two separate operators.

Histopathological analysis of mice BM. Sections of WT and $p50^{-/-}$ BM were routinely stained with Haematoxylin and Eosin (H&E) and analyzed by an expert pathologist (CT) using a Leica DM2000 optical microscope (x400 and x630 magnification) and microphotographs were collected with a Leica DFC320 digital camera using the Leica IM50 imaging software.

Quantification of circulating granulocytes in peripheral blood smears. Cell counts were visually performed on five May-Grunwald Giemsa-stained smears on high-power microscopic fields (x400 magnification) and the average number of total and immature granulocytes was determined by averaging the counts.

Flow cytometry and sorting. Splenocytes were collected from spleen after disaggregation and filtration through Falcon strainers (70 µm). Primary tumors were cut into small pieces, disaggregated with 0.5 mg ml^{-1} collagenase IV and 150 U ml^{-1} DNase I in RPMI-1640 for 30 min at 37 °C and filtered through strainers. Cells ($10^{\wedge 6}$) were re-suspended in HBSS (Hank's balanced salt solution, Lonza) supplemented with 0.5% BSA (Sigma) and the staining was performed at 4°C for 20 minutes with specific antibodies. (detailed information is provided in the supplementary materials and methods). Cells were analyzed using the BD FACSCanto™ II or BD LSRFortessa™ and BD FACSDiva and FlowJo (9.3.2) software.

mRNA Sequencing (mRNA-Seq) Total RNA was extracted from 1-5*10^6 M-MDSC (RNeasy kit, Quiagen), and 2-5 µg were used to generate sequencing libraries with a Truseq RNA Sample Prep Kit V2 (Illumina) according to the manufacturer's instructions. Sequencing was performed on a HiSeq2000

(Illumina).

Chromatin Immunoprecipitation (ChIP). ChIP was carried out with a previously described high-throughput protocol (30,31). Details are reported in the supplementary Materials & Methods.

Computational methods: computational analysis of data generated by RNA-SEQ and ChIP-SEQ is described in the supplemental experimental procedures.

Confocal microscopy on BM-MDSC, spleen MDSC and PEC. Cells were seeded on Poly-L-Lysine (Sigma-Aldrich) coated sterile rounded glasses at $2x10^5$ cells/ml in medium and fixed with 4% PFA for 10 minutes at room temperature. Cell staining and analysis are described in supplementary Material & Methods.

Statistics. Statistical significance between two groups was determined by two-tailed Student's *t* test or two way ANOVA corrected for multiple comparison by Sidak's test and among more than two groups by one-way or two-way ANOVA corrected for multiple comparison by Tukey's test (Prism version 6). *p <0.05; ** p <0.01; *** p <0.001.

Real time PCR analysis, MTT assay, Enzyme-linked Immunosorbent Assay (ELISA) are described in the supplementary Materials & Methods

RESULTS

p50 NF-κB controls both M-MDSC suppressive functions and differentiation of myeloid precursors.

Nuclear accumulation of p50 NF-κB, as occurring in TAMs and LPS-tolerant macrophages, impairs both M1 polarization and antitumor activities (9,10). Similar to TAMs, confocal microscopy analysis showed selective nuclear accumulation of p50 NF-κB in splenic and tumor-infiltrating monocytic (M) – MDSCs ($CD11b^{+}Ly6G^{-}Ly6C^{+}$ cells) from fibrosarcoma (MN/MCA1) bearing mice, at advanced stages of tumor development (day 21; **Fig. 1A, Supplementary Fig. S1A**). As inhibition of T cells proliferation validated the suppressive activity of these cells (**Supplementary Fig. S1B**), we explored whether p50 NF-κB could be actually involved in accumulation of suppressive M-MDSC occurring during tumor development. According to our previous findings (10,27), C57BL/6 $p50^{-/-}$ mice displayed both reduced tumor growth and metastasis formation, as compared to WT mice (**Fig. 1B**) but, paradoxically, displayed increased accumulation of splenic and tumor myeloid cells expressing the M-MDSCs phenotype $CD11b^{+}Ly6G^{-}Ly6C^{+}$ (**Fig. 1C-D and Supplementary Figure S1C**). Of note this event coincided temporally with the nuclear accumulation of p50, as observed in WT mice (21 days) (**Fig. 1A**). Cells expressing the PMN-MDSCs phenotype $CD11b^{+}Ly6G^{+}Ly6C^{low/-}$ also accumulated during disease progression (**Fig. 1C-D and Supplementary Figure S1C**), however without exhibiting nuclear accumulation of p50 NF-κB (**Fig. 1A and Supplementary Fig. S1A**). Hence, we analyzed whether p50 could affect the expression of genes encoding for immunosuppressive activities (12,32). Noteworthy, in the absence of p50, magnetically sorted splenic $CD11b^{+}Ly6G^{-}Ly6C^{+}$ cells (**Supplementary Fig. S1D**) showed a drastic reduction of both *Nos2* gene expression (**Fig. 1E**) and NO production (**Fig. 1F**), in response to IFNγ treatment. Accordingly, p50

depletion impaired *in vivo* NO production in tumor tissues (**Supplementary Fig. S1E**). In contrast, both *Nos2* mRNA (**Fig. 1E**) and NO production (**Fig. 1F**) were poorly induced by IFNγ treatment in both WT and $p50^{-/-}$ splenic $CD11b^{+}Ly6G^{+}Ly6C^{low/-}$ cells (**Supplementary Fig. S1D**). Furthermore the expression of arginase I (*Arg1*) (13), indoleamine-2,3-dioxygenase (*Ido1*), and Programmed Cell Death 1 Ligand 1 (*CD274*) were poorly affected by the lack of p50 in both splenic and tumor $CD11b^{+}Ly6G^{-}Ly6C^{+}$ and $CD11b^{+}Ly6G^{+}Ly6C^{low/-}$ cells (**Supplementary Fig. S1F-G**) and not further investigated. To establish the actual role of p50 NF-κB in the suppressive activity of both myeloid subsets, $CD11b^{+}Ly6G^{-}Ly6C^{+}$ and $CD11b^{+}Ly6G^{+}Ly6C^{low/-}$ cells were isolated from tumor and spleen of fibrosarcoma (MN/MCA1)-bearing mice, activated with IFNγ and tested for their ability to inhibit T cell proliferation. Consistently, both splenic and tumor M-MDSC from WT mice strongly inhibited T cell proliferation, whereas the p50-deficient counterparts displayed impaired suppressive ability (**Fig 1G, 1H**).

In accordance with the lack of p50 nuclear accumulation, $CD11b^{+}Ly6G^{+}Ly6C^{low/-}$, both WT and p50-deficient, showed no suppressive activity (**Fig 1G, 1H**). To further characterize the mechanisms underpinning the suppressive activity of p50 NF-κB, splenic M-MDSCs isolated from tumor bearing mice were activated with IFNγ and tested for antigen-specific suppressive activity. In keeping with the data above, $p50^{-/-}$ M-MDSC displayed reduced suppressive activity (**Fig. 1I, left**), and NO levels in the co-culture supernatants (**Fig. 1I, right**). The M-MDSC suppressive activity was NO-dependent, as addition of the NOS inhibitor L-NMMA to the co-culture

abolished both T cell suppression (**Fig. 1I, left**) and NO production (**Fig. 1I, right**). These data suggested that the NO-dependent suppressive capacity of M-MDSCs in response to IFNγ, relies on p50 nuclear accumulation. We next determined whether the nuclear accumulation of p50 was also observable in blood M-MDSCs (13, 33) from colorectal carcinoma patients (CRC). Compared to healthy donors, the frequency of M-MDSC ($CD33^{+}CD14^{+}HLA\text{-}DR^{low/-}$) was increased and these cells expressed higher level of NOS2 (**Figure 1J and Supplementary Fig. S2A**), as well as increased nuclear levels of p50 **(Fig. 1K)**, as compared to peripheral blood mononuclear $CD14^{+}$ cells from healthy donors. To confirm the role of p50 in human myeloid cells, circulating $CD14^{+}HLA\text{-}DR^{+}$ mononuclear cells from healthy donors were transfected with a small interfering RNA against p50 (p50 siRNA). Silencing of p50 (**Supplementary Fig. S2B**), significantly inhibited *NOS2* mRNA expression in response to IFNγ treatment (**Supplementary Figure S2C**).

The predominant increase in the M-MDSCs subset within the spleen of tumor-bearing mice might results from its accelerated proliferation rate or preferential skewing of precursors. To study the implication of p50 in either normal or emergency hematopoiesis, we first evaluated the BM of naïve mice for composition in hematopoietic stem cells (HSC), along with their proliferation and differentiation potential. HSCs are immunophenotypically defined as cells lacking lineage specific markers (Lin-) but expressing Sca-1 and c-Kit (Lin-Sca-1+c-kit+, LSK), while the methylcellulose based colony-forming unit (CFU) assay allows to quantify their derived progeny *in vitro*. We observed a significant enrichment of LSK progenitors (Lin-Sca-1+c-kit+) in BM of $p50^{-/-}$ mice (**Fig. 2A, B**), associated with higher clonogenic potential of $p50^{-}$

$^{/-}$ HSCs in both GM-CFU and M-CFU progenitors, but not in G-CFU (**Fig. 2C**). These results indicate that lack of p50 results in a preferential skewing of HSC towards the monocytic branch at the myeloid/granulocytic bifurcation. Accordingly, histopathological analysis showed a severe impairment of terminal granulopoiesis in the BM of $p50^{-/-}$ mice, which was associated with an increased number of immature myeloid precursors (**Fig. 2D**). Consistently, the hematopoietic parenchyma of $p50^{-/-}$ mice was characterized by the marked reduction of mature segmented granulocytes and by the expansion of myeloid blasts showing abnormal interstitial localization and aggregation in clusters **(Fig. 2D)**. Monocytic differentiation (**Fig. 2E**) was preserved in the BM of $p50^{-/-}$ mice. Consistent with BM histopathology, flow cytometry revealed a neat decrease in the $Gr1^{+}$c-Kit^{-} granulocytic population and a paralleled increase in $Gr1^{+}$c-kit^{+} myeloblasts in $p50^{-/-}$, as compared to control WT BM (**Fig. 2F**). Accordingly, blood granulocytes from $p50^{-/-}$ mice were enriched in immature and blast-like forms compared with circulating granulocytes from WT controls (**Fig. 2G**). Overall, these results confirm previous observations (34) and demonstrate that p50 NF-κB deficiency is associated with defective granulocytic differentiation in favor of the monocytic lineage. Lack of p50 resulted in a significant accumulation of LSK progenitors (Lin-Sca-1^{+}c-kit^{+}) also in the BM of tumor bearers (**Fig 2H**). Furthermore, both histopathology (**Fig 2I**) and flow cytometry (**Fig 2J**) of BM confirmed the reduction of the mature $Gr1^{+}$c-kit^{-} and the concomitant increase of the immature $Gr1^{+}$c-kit^{+} granulocytic cells in $p50^{-/-}$ tumor bearers. Of relevance, cytofluorimetric analysis of tumor infiltrating MDSC revealed a significant increase of the negative regulator of MDSC expansion IRF8 (35) expression by the p50-

deficient PMN-MDSC subset ($CD11b^+Ly6G^+$ cells) (**Fig. 2K**), which also acts as promoter of terminal monocytic maturation (36). This result is in agreement with the preferential expansion of non-suppressive $Ly6C^+$ monocytic cells (M-MDSC-like) observed in tumor bearing p50-deficient mice.

Hematopoietic deletion of p50 NF-κB abolishes NO production by M-MDSCs and impairs metastasis formation

To establish whether the expression of p50 NF-κB in the hematopoietic compartment was uniquely responsible for the suppressive activity of M-MDSCs, we generated chimeric mice by transplanting WT or $p50^{-/-}$ BM cells into sub-lethally irradiated WT and $p50^{-/-}$ mice, which were subsequently implanted with the MN/MCA1 fibrosarcoma. Splenic $CD11b^+Ly6G^-Ly6C^+$ cells isolated from mice receiving $p50^{-/-}$ BM cells, and subsequently activated with IFNγ, were strongly impaired in their capacity to suppress both T cell proliferation and NO production (**Fig. 3A**). To investigate further the *in vivo* importance of p50 in the hematopoietic compartment, we used the deleter strain B6.Cg-Tg(Tek-Cre)1Ywa to ablate p50 in all hematopoietic lineage cells ($p50^{Tie2}$ mice) (37). In agreement with **Fig. 1A** and **B**, we observed inhibition of lung metastasis formation in tumor bearing $p50^{Tie2}$ mice, which was paralleled by an increased number of splenic and tumor infiltrating $CD11b^+$ $Ly6G^-Ly6C^{high}$ cells, while an increase of $CD11b^+Ly6C^{low/-}Ly6G^+$ cells was observed at the tumor site (**Fig. 3B**).

Further, splenic and tumor-associated $CD11b^+Ly6G^-Ly6C^+$ cells from $p50^{Tie2}$ mice (**Fig. 3C**) showed decreased NOS2 but higher TNFα expression,

366 associated with increased number of both splenic and tumor-infiltrating IFNγ
367 expressing $CD4^+$ and $CD8^+$ T cells (**Fig. 3D**), these latter also expressing high
368 levels of the cytotoxic molecule Granzyme B (GZMB). Accordingly,
369 $CD11b^+Ly6G^-Ly6C^+$ cells isolated from $p50^{Tie2}$ mice showed a reduced ability
370 to inhibit T cells proliferation, whereas $CD11b^+Ly6G^+Ly6C^{Low/-}$ cells lacked
371 suppressive activity (**Fig 3E**). Of note, transplantation of B16 melanoma cells
372 (38) in $p50^{Tie2}$ mice fully recapitulated the phenotype of the MN-MCA1
373 fibrosarcoma, both in terms of tumor growth **(Supplementary Fig. S3A)** and
374 accumulation of splenic and tumor infiltrating immune cells (**Supplementary**
375 **Fig. S3B, C, D**).

376

377 **p50 influences IFNγ-induced Stat1 recruitment to a subset of p50-**
378 **dependent genes**

379 Since the absence of p50 has strongly altered the response of $CD11b^+Ly6G^-$
380 $Ly6C^+$ cells to IFNγ, we further investigated this aspect. IFNγ-induced Stat1
381 phosphorylation (39) was not reduced in the absence of p50 (**Fig. 4A**)
382 suggesting that downstream events occurring in $p50^{-/-}$ cells could be
383 responsible for defective IFNγ-mediated gene expression. To directly assess
384 this hypothesis, we generated mRNA sequencing (mRNA-Seq) data sets of
385 WT and $p50^{-/-}$ $CD11b^+Ly6G^-Ly6C^+$ cells, isolated from the spleen of tumor
386 bearing mice, treated or not with IFNγ. $p50^{-/-}$ $CD11b^+Ly6G^-Ly6C^+$ cells showed
387 selective gene expression defects in response to IFNγ stimulation as
388 compared to WT controls (**Fig. 4B and Supplementary Table 1**). Using as

cutoffs a log2(fold change) ≥ 1 and a FDR ≤ 0.05, 15 (2.4%, cluster 2) of the 628 genes induced by IFNγ in WT $CD11b^{+}Ly6G^{-}Ly6C^{+}$ cells *15 (2.38%)* were down-regulated in $p50^{-/-}$ cells, whereas 16 (2.5%) were up-regulated. Analysis of the generated gene profiles confirmed that p50 deficiency results in a significant impaired induction of *Nos2* (**Fig. 4C**) along with an increased induction of some interferon inducible genes, such as Oas1g and Pyhin1/Ifix, (**Supplementary Table 1**). Collectively, our data highlight a specific function of p50 in controlling a subset of functionally relevant genes in response to IFNγ stimulation. Since transcriptional responses to IFNγ predominantly rely on the Stat1 transcription factor, we evaluated the recruitment of Stat1 on the Nos2 gene using Chromatin Immunoprecipitation (ChIP) with a validated antibody directed against Stat1 (30). Lack of p50 reduced binding of Stat1 on the Nos2 gene in $CD11b^{+}Ly6C^{high}$ cells under both steady state and IFNγ treatment (**Fig. 4D**), therefore indicating that p50 controls IFNγ-dependent responses at epigenetic level.

Along with MDSCs, macrophages produce NO in response to IFNγ, which mediate either their immunosuppressive (4,13) or tumoricidal capacity (40). Similar to M-MDSCs, in thioglycollate elicited macrophages (PECs) lack of p50 decreased *Nos2* mRNA expression and NO production in response to IFNγ (**Supplementary Fig. S4A**), without reducing Stat1 phosphorylation (**Supplementary Fig. S4B)**. In further analogy with MDSCs, PECs primed with the tumor supernatant (TSN) produced higher level of NO in response to IFNγ, in a p50-dependent manner (**Supplementary Fig. S4C**). Moreover, transcriptional analysis (mRNA-Seq) of WT and $p50^{-/-}$ PECs confirmed that $p50^{-/-}$ PECs showed selective gene expression defects in response to IFNγ

(**Supplementary Fig. S4D** and **Supplementary Table 2**), including *Nos2.* On the other hand, in agreement with **Fig. 2H**, p50 deficiency resulted in an increased induction of the monopoiesis-inducing transcription factor *Irf8* (36) (**Supplementary Table 2**). We then performed ChIP coupled to next-generation sequencing (ChIP-Seq). Almost all DNA binding events occurred only after Stat1 activation (**Supplementary Table 3**) and positively correlated with IFNγ-induced gene expression in a statistically significant manner (**Supplementary Fig. S4E**), highlighting the prominent role of Stat1 as a transcriptional activator. A discrete fraction of the Stat1 cistrome was selectively affected by p50 deficiency, with an abrogation or reduction of Stat1 occupancy at 2571 sites (8.3% of all inducible peaks) in $p50^{-/-}$ PEC relative to WT controls. For instance, we confirmed that Stat1 was not efficiently recruited to either promoters or enhancers of *Nos2* gene in $p50^{-/-}$ macrophages, and this was associated with its reduced induction in response to IFNγ (**Supplementary Fig. S4F)**. These observations were then validated at a genomic scale by computationally integrating our ChIP-Seq and mRNA-Seq datasets (**Supplementary Table 4**). As shown in **Supplementary Fig. S4G**, p50-dependent genes were located at shorter distances from p50-dependent Stat1 peaks than p50-independent genes. Conversely, p50-independent genes were closer to p50-independent Stat1 peaks.

These findings identify a role for p50 in controlling IFNγ-induced *Nos2* gene expression in myeloid cells, and are consistent with a model of p50-dependent assistance of Stat1 recruitment to selected p50-dependent genes in response to IFNγ treatment.

438

439 **Ablation of p50 NF-κB in M-MDSCs restores the *in vivo* antitumor**
440 **activity of IFNγ**

441 We next investigated whether increased nuclear p50 NF-κB in M-MDSCs
442 limits cytokine-mediated immunotherapy *in vivo.* While IFNγ treatment of WT
443 tumor-bearing mice was ineffective, the same treatment significantly reduced
444 tumor development in $p50^{-/-}$ mice (**Fig. 5A)**. Noteworthy, *in vivo* depletion of
445 $CD4^+$ and $CD8^+$ T cells in p50 NF-κB-deficient tumor bearing mice restored
446 tumor growth (**Fig. 5A, center**) and metastasis formation (**Fig. 5A, right**),
447 indicating that myeloid-specific p50 NF-κB is suppressing specific antitumor
448 immunity. Hence, to test the specific contribution of p50 to the
449 immunosuppressive activity of M-MDSCs, $p50^{-/-}$ tumor-bearing mice were
450 adoptively transferred with WT M-MDSCs ($1x10^6$) and treated daily with IFNγ.
451 Such M-MDSCs transfer restored tumor growth in $p50^{-/-}$ mice (**Fig. 5B**) and
452 decreased both IFNγ production and GZMB expression by $CD8^+$ T cells, both
453 in the spleen and the primary tumor (**Fig. 5C,D**). Of note, transfer of $p50^{-/-}$
454 $CD11b^+Ly6G^-Ly6C^+$ cells did not affect tumor growth, as well as the
455 phenotype of $CD4^+$ and $CD8^+$ T cells. These data demonstrate that
456 accumulation of nuclear p50 in M-MDSCs promotes their suppressive
457 functions in blunting the efficacy of cytokine-mediated immunotherapy (i.e.
458 IFNγ). This conclusion was further strengthened observing that ablation of p50
459 in tumor bearing mice improved the antitumor and anti-metastatic activity of
460 the immunostimulatory cytokine IL-12 (**Supplementary Fig. S5**).

Tumor-derived PGE2 primes M-MDSCs for higher IFNγ-induced NO-mediated suppressive activity

In the attempt to identify tumor-derived signals controlling nuclear p50 accumulation, we used BM-MDSC (29) to test molecules detected in the tumor supernatants (TSN) (**Fig. 6A**) and reported to either induce nuclear accumulation of p50 NF-κB homodimers in macrophages (i.e. PGE2, IL-10, TGFβ)(10) or myeloid cell differentiation (GM-CSF, G-CSF and M-CSF). Confocal microscopy analysis showed that neither M-, GM- nor G-CSF induced p50 accumulation (**Supplementary Fig. S6A**). In contrast, PGE2 efficiently induced nuclear p50, whereas the PGE2 receptor antagonists EP2 (AH6809) and EP4 (AH23848) (41) inhibited the TSN-induced nuclear accumulation of p50 (**Fig. 6B**). Furthermore, BM-MDSCs primed with TSN showed higher levels of both *Nos2* mRNA and NO production in response to IFNγ (**Fig. 6C**), which was prevented by AH6809 (**Fig. 6D**). In agreement, pretreatment with Butaprost, a selective agonist of EP2, enhanced IFNγ-mediated NO production in a p50-dependent manner (**Fig. 6D**).

We next evaluated the capacity of AH6809 to interfere with the MN/MCA1 fibrosarcoma *in vivo*. Since MN-MCA1 cells also express the EP2R (**Supplementary Fig. S6B**), we evaluated the effects of AH6809 on tumor cell viability. MN-MCA1 cells were cultured in presence of 10μM AH6809, 10μM PGE2 or the combination of AH6809 and PGE2, up to 72 hours. As shown (**Supplementary Fig. S6C**), AH6809 did not affect tumor cell proliferation and viability. In contrast, daily treatment with AH6809 inhibited tumor growth (**Fig.**

485 **6E, left**) and reduced the number of lung metastasis (**Fig. 6E, right**) in WT
486 mice. Consistently, no tumor growth inhibition was observed in $p50^{-/-}$ mice
487 upon treatment with AH6809 (**Fig. 6E, left**). In agreement with the phenotype
488 of $p50^{-/-}$ mice (**Fig. 3C,D**), flow cytometry of tumor tissue (MN/MCA1) from
489 tumor bearing WT mice, showed that AH6809 treatment significantly reduced
490 the expression of NOS2 (**Fig. 6F, left**) by $CD11b^{+}Ly6G^{-}Ly6C^{+}$ cells, while
491 increasing the expression of TNFα (**Fig. 6F, center**), as well as the
492 $IFN\gamma^{+}CD4^{+}$ and $IFN\gamma^{+}CD8^{+}$ T cells (**Fig. 6F, right**). Similar results were
493 obtained in splenic M-MDSCs (**Fig. 6G**). Further supporting the protumoral
494 activity of the PGE2-p50-NO axis, *in vivo* treatment with AH6809 displayed an
495 antitumor effects comparable with an antibody against the PD-1 immune
496 checkpoint inhibitor (anti-PD-1), both in terms of primary tumor growth
497 (MN/MCA1) and lung metastasis formation (**Supplementary Fig. S6D**), while
498 the expression of NOS2 in $CD11b^{+}Ly6C^{+}$ WT M-MDSCs cells was reduced to
499 levels comparable with $p50^{-/-}$ M-MDSC (**Supplementary Fig S6E**). In
500 agreement, treatment of B16 bearing WT mice with AH6809 reduced tumor
501 growth and NOS2 expression by $CD11b^{+}Ly6C^{+}$ M-MDSC, mimicking p50 NF-
502 κB ablation (**Supplementary Fig. S6F**). Despite also B16 melanoma cells
503 expressed EP2R (**Supplementary Fig. S6G**), AH6809 did not elicit direct
504 cytotoxic effects *in vitro* (**Supplementary Fig. S6H**), neither antitumor effects
505 in p50-deficient mice (**Supplementary Fig. S6F**).

506 Finally, we investigated the effect of NO on the antitumor activity of IFNγ *in*
507 *vivo*. WT B16-bearing mice were then treated with IFNγ and/or with L-NMMA.
508 While treatment with IFNγ elicited poor effects on tumor growth, L-NMMA

alone displayed a significant antitumor effect, which was enhanced in combination with IFNγ (**Fig. 7A**). Moreover, L-NMMA, and even more its combination with IFNγ, reduced the expression of NOS2 by tumor M-MDSC (**Fig. 7B, top**) and enhanced the expression of TNFα (**Fig. 7B, bottom**), while increasing the number of tumor-infiltrating $IFN\gamma^{+}CD8^{+}$ T cells (**Fig. 7C**). These results indicate NO as a terminal mediator of suppressive myeloid cell functions and suggest that blocking the PGE2-p50-NO axis either upstream (i.e. EP2 inhibitors) or downstream (ie. NOS2 inhibitor L-NMMA) may restore antitumor immunity.

To corroborate this finding in cancer patients, we analyzed the expression of both the PGE2 receptor EP2 and NOS2 in PBMCs from patients with advanced colorectal cancer (CRC; stage T2/T3; n = 5). In agreement with mouse data, human M-MDSCs ($HLA\text{-}DR^{low/-}CD14^{+}CD33^{high}$) (**Supplementary Fig. S2A)** expressed the PGE2 receptor EP2 (**Fig. 7D**). Moreover, human peripheral blood monocytes primed with TSN from the human pancreatic carcinoma cell line PANC1, containing 923 µg/ml of PGE2, and subsequently treated with IFNγ, showed higher levels of intracellular NOS2 protein, that were reduced by treatment with AH6809 (**Fig. 7E**). While confirming the suppressive activity of PGE2 in cancer bearers (42), our results are the first to identify the PGE2-driven nuclear accumulation of p50 NF-κB as leading event in the differentiation of suppressive M-MDSCs.

DISCUSSION

Cancers support a pathological generation of immunosuppressive and tumor-promoting MDSC populations (12,13), that share phenotypic traits with TAMs,

including the expression of anti-inflammatory M2 polarized genes (10). Here, we demonstrate that tumor-derived PGE2 drives the suppressive phenotype of M-MDSCs through upregulation of nuclear p50 NF-κB, a key player in the resolution of the inflammatory response, that links unresolved cancer-inflammation with tolerance (9,28). Accumulation of nuclear p50 NF-κB, in both mouse ($CD11b^{+}Ly6G^{-}Ly6C^{+}$) and human (CRC patients) ($CD14^{+}HLA\text{-}DR^{low/-}$) M-MDSCs, diverts their transcriptional responses to IFNγ towards enhanced production of the immunosuppressive molecule NO. Consistently, ablation of p50 NF-κB reactivated specific antitumor immunity and reinstated the *in vivo* antitumor activity of IL-12 and IFNγ, two immunostimulatory cytokines evaluated in clinical trials against various human tumors (e.g. CRC, soft tissue sarcoma, melanoma and plasma cell neoplasms) (16). This observation provides new insights into the ambivalent action of IFNγ (22,43,44), which in clinical protocols has shown either moderate or poor efficacy (17,21,45). This ambiguity is reminiscent of the bimodal immunological activities of IFNγ, which promotes transcription of genes involved in the activation of immune responses (eg. MHC class I and class II, IL-12) (46) and simultaneously induces immunosuppressive pathways, including B7-H1 (47,48) and the immunosuppressive enzymes IDO (23) and iNOS/NOS2 (12,13). The biological activity of IFNγ requires the nuclear translocation and the DNA binding of the STAT1 homodimer to gamma activated sequence (GAS) sites on the promoters of downstream target genes (49), including Nos2 (50). Accumulation of p50 NF-κB in myeloid cells does not affect IFNγ-dependent STAT1 phosphorylation, but rather controls their chromatin landscape to promote binding of STAT1 onto specific gene

regulatory elements of IFNγ-responsive genes, including *Nos2*. We also observed that lack of p50 results in increased $CD11b^{+}Ly6G^{-}Ly6C^{+}$ cells in the spleen of tumor-bearing mice, with low NO production and suppressive activity, as well as in the preferential skewing of HSCs towards the monocytic branch in the bone marrow. This hematopoietic output is in agreement with the $Irf8^{high}$ feature that we observed in p50-deficient PMN-MDSCs, since IRF8 is a cell fate switching factor driving terminal differentiation of the monocytic lineage (36) ad preventing MDSC expansion (35).

COX2-stimulated production of PGE2 enhances the expansion of MDSCs and promotes suppression of adaptive immunity (51). We show that antagonists of the PGE2 receptors EP1/EP2 reprogram M-MDSC functions in response to IFNγ towards an inflammatory phenotype (i.e. $NOS2^{low}/TNF^{high}$), associated with increased specific anti-tumor immunity. Of relevance, in analogy with the results obtained both with the inhibition of PGE2 receptors and with the ablation of the NF-κB p50 gene, the NOS L-NMMA inhibitor reprogrammed the M-MDSCs towards towards an $NOS2^{low}/TNF\alpha^{high}$ phenotype, associated with an increased antitumoral effect of IFNγ. This evidence indicates the gasotransmitter NO (52) as the final effector of the protumoral reprogramming of myeloid cells, guided by the PGE2 / p50 axis.

COX inhibitors (e.g. aspirin) were suggested for prevention and treatment of cancer (42). Nevertheless, due to their severe side effects, targeting specific prostanoid receptors endowed with immunosuppressive properties, such as EP2 (53-55), might provide an alternative selective and safer approach to burst specific immunity in cancer patients. Our work indicates that p50 NF-κB

accumulation diverts the differentiation and activation status of myeloid cells, leading to the resolution of immune and inflammatory responses. It further demonstrates that in cancer an accumulation of p50 NF-κB, induced by PGE2, acts as an epigenetic hacker of M-MDSC functions, which establishes their suppressive phenotype, suggesting the use of PGE2 receptor antagonists as potential adjuvants for anticancer immunotherapy.

ACKNOWLEDGMENTS

This work was supported by Associazione Italiana per la Ricerca sul Cancro (AIRC) Italy (My First Grant number 12810 to S.S.; IG numbers 10137 to MPC; IG numbers 15585, 19885 to A.S.; AIRC 5 per Mille, number 22757 to AS; AIRC 5 per Mille, Program Innovative Tools for Cancer Risk Assessment and Diagnosis, number 12162 to CT; Three-Year fellowship “Pierluigi Meneghelli”, project code 19682 to F.M.C.). Ministero dell’istruzione, dell’Università e della Ricerca (MIUR), Italy (PRIN 2015YYKPNN and 2017BA9LM5_001 to A.S.); Ministero della Salute, Ricerca Finalizzata RF-2016-0236842 to A.S. and GR-2013-02355637 to S.S; European Research Council (ERC) Advanced grant ERCAdGN.692789 to G.N.; Fondazione Cariplo 2016/0871 to A.S., Associazione “Augusto per la Vita”, Novellara, Italy, to A.S., Associazione “Medicine Rocks”, Milan, Italy to A.S. and Università del Piemonte Orientale, Novara, Italy, Ricerca locale 2019 to C.P.

606

607

608 **REFERENCES**

609 1. Mosser DM, Edwards JP. Exploring the full spectrum of macrophage
610 activation. Nat Rev Immunol **2008**;8:958-69
611 2. Sica A, Mantovani A. Macrophage plasticity and polarization: in vivo
612 veritas. J Clin Invest **2012**;122:787-95
613 3. Mantovani A, Sozzani S, Locati M, Allavena P, Sica A. Macrophage
614 polarization: tumor-associated macrophages as a paradigm for polarized
615 M2 mononuclear phagocytes. Trends Immunol **2002**;23:549-55
616 4. Mantovani A, Sica A. Macrophages, innate immunity and cancer: balance,
617 tolerance, and diversity. Curr Opin Immunol **2010**;22:231-7
618 5. Mantovani A, Allavena P, Sica A, Balkwill F. Cancer-related inflammation.
619 Nature **2008**;454:436-44
620 6. Martinez FO, Helming L, Gordon S. Alternative activation of macrophages:
621 an immunologic functional perspective. Annu Rev Immunol **2009**;27:451-
622 83
623 7. Noy R, Pollard JW. Tumor-associated macrophages: from mechanisms to
624 therapy. Immunity **2014**;41:49-61
625 8. Ziegler-Heitbrock HW, Petersmann I, Frankenberger M. p50 (NF-kappa
626 B1) is upregulated in LPS tolerant P388D1 murine macrophages.
627 Immunobiology **1997**;198:73-80
628 9. Porta C, Rimoldi M, Raes G, Brys L, Ghezzi P, Di Liberto D, et al. Tolerance
629 and M2 (alternative) macrophage polarization are related processes
630 orchestrated by p50 nuclear factor kappaB. Proc Natl Acad Sci U S A
631 **2009**;106:14978-83
632 10. Biswas SK, Gangi L, Paul S, Schioppa T, Saccani A, Sironi M, et al. A distinct
633 and unique transcriptional program expressed by tumor-associated
634 macrophages (defective NF-kappaB and enhanced IRF-3/STAT1
635 activation). Blood **2006**;107:2112-22
636 11. Strauss L, Sangaletti S, Consonni FM, Szebeni G, Morlacchi S, Totaro MG, et
637 al. RORC1 Regulates Tumor-Promoting "Emergency" Granulo-
638 Monocytopoiesis. Cancer Cell **2015**;28:253-69
639 12. Sica A, Bronte V. Altered macrophage differentiation and immune
640 dysfunction in tumor development. J Clin Invest **2007**;117:1155-66
641 13. Gabrilovich DI, Ostrand-Rosenberg S, Bronte V. Coordinated regulation of
642 myeloid cells by tumours. Nat Rev Immunol **2012**;12:253-68
643 14. Martin F, Apetoh L, Ghiringhelli F. Role of myeloid-derived suppressor
644 cells in tumor immunotherapy. Immunotherapy **2012**;4:43-57
645 15. Zaidi MR, Davis S, Noonan FP, Graff-Cherry C, Hawley TS, Walker RL, et al.
646 Interferon-gamma links ultraviolet radiation to melanomagenesis in mice.
647 Nature **2011**;469:548-53
648 16. Vacchelli E, Galluzzi L, Eggermont A, Galon J, Tartour E, Zitvogel L, et al.
649 Trial Watch: Immunostimulatory cytokines. Oncoimmunology
650 **2012**;1:493-506

17. Miller CH, Maher SG, Young HA. Clinical Use of Interferon-gamma. Ann N Y Acad Sci **2009**;1182:69-79
18. Assi HI, Kamphorst AO, Moukalled NM, Ramalingam SS. Immune checkpoint inhibitors in advanced non-small cell lung cancer. Cancer **2018**;124:248-61
19. Lo Russo G, Moro M, Sommariva M, Cancila V, Boeri M, Centonze G, et al. Antibody-Fc/FcR Interaction on Macrophages as a Mechanism for Hyperprogressive Disease in Non-small Cell Lung Cancer Subsequent to PD-1/PD-L1 Blockade. Clin Cancer Res **2019**;25:989-99
20. Adams DO, Hamilton TA. The cell biology of macrophage activation. Annu Rev Immunol **1984**;2:283-318
21. Zaidi MR, Merlino G. The two faces of interferon-gamma in cancer. Clin Cancer Res **2011**;17:6118-24
22. Dighe AS, Richards E, Old LJ, Schreiber RD. Enhanced in vivo growth and resistance to rejection of tumor cells expressing dominant negative IFN gamma receptors. Immunity **1994**;1:447-56
23. Pallotta MT, Orabona C, Volpi C, Vacca C, Belladonna ML, Bianchi R, et al. Indoleamine 2,3-dioxygenase is a signaling protein in long-term tolerance by dendritic cells. Nat Immunol **2011**;12:870-8
24. Kondo A, Yamashita T, Tamura H, Zhao W, Tsuji T, Shimizu M, et al. Interferon-gamma and tumor necrosis factor-alpha induce an immunoinhibitory molecule, B7-H1, via nuclear factor-kappaB activation in blasts in myelodysplastic syndromes. Blood **2010**;116:1124-31
25. Topalian SL, Drake CG, Pardoll DM. Immune checkpoint blockade: a common denominator approach to cancer therapy. Cancer Cell **2015**;27:450-61
26. Chan SR, Vermi W, Luo J, Lucini L, Rickert C, Fowler AM, et al. STAT1-deficient mice spontaneously develop estrogen receptor alpha-positive luminal mammary carcinomas. Breast Cancer Res **2012**;14:R16
27. Saccani A, Schioppa T, Porta C, Biswas SK, Nebuloni M, Vago L, et al. p50 nuclear factor-kappaB overexpression in tumor-associated macrophages inhibits M1 inflammatory responses and antitumor resistance. Cancer Res **2006**;66:11432-40
28. Porta C, Ippolito A, Consonni FM, Carraro L, Celesti G, Correale C, et al. Protumor Steering of Cancer Inflammation by p50 NF-kappaB Enhances Colorectal Cancer Progression. Cancer Immunol Res **2018**;6:578-93
29. Marigo I, Bosio E, Solito S, Mesa C, Fernandez A, Dolcetti L, et al. Tumor-induced tolerance and immune suppression depend on the C/EBPbeta transcription factor. Immunity **2010**;32:790-802
30. Ostuni R, Natoli G. Lineages, cell types and functional states: a genomic view. Curr Opin Cell Biol **2013**;25:759-64
31. Garber M, Yosef N, Goren A, Raychowdhury R, Thielke A, Guttman M, et al. A high-throughput chromatin immunoprecipitation approach reveals principles of dynamic gene regulation in mammals. Mol Cell **2012**;47:810-22
32. Movahedi K, Guilliams M, Van den Bossche J, Van den Bergh R, Gysemans C, Beschin A, et al. Identification of discrete tumor-induced myeloid-derived suppressor cell subpopulations with distinct T cell-suppressive activity. Blood **2008**;111:4233-44

33. Mandruzzato S, Solito S, Falisi E, Francescato S, Chiarion-Sileni V, Mocellin S, et al. IL4Ralpha+ myeloid-derived suppressor cell expansion in cancer patients. J Immunol **2009**;182:6562-8
34. Wang D, Paz-Priel I, Friedman AD. NF-kappa B p50 regulates C/EBP alpha expression and inflammatory cytokine-induced neutrophil production. J Immunol **2009**;182:5757-62
35. Waight JD, Netherby C, Hensen ML, Miller A, Hu Q, Liu S, et al. Myeloid-derived suppressor cell development is regulated by a STAT/IRF-8 axis. J Clin Invest **2013**;123:4464-78
36. Friedman AD. Transcriptional control of granulocyte and monocyte development. Oncogene **2007**;26:6816-28
37. El Kasmi KC, Qualls JE, Pesce JT, Smith AM, Thompson RW, Henao-Tamayo M, et al. Toll-like receptor-induced arginase 1 in macrophages thwarts effective immunity against intracellular pathogens. Nat Immunol **2008**;9:1399-406
38. Sica A, Saccani A, Bottazzi B, Polentarutti N, Vecchi A, van Damme J, et al. Autocrine production of IL-10 mediates defective IL-12 production and NF-kappa B activation in tumor-associated macrophages. J Immunol **2000**;164:762-7
39. Platanias LC. Mechanisms of type-I- and type-II-interferon-mediated signalling. Nat Rev Immunol **2005**;5:375-86
40. Dinapoli MR, Calderon CL, Lopez DM. The altered tumoricidal capacity of macrophages isolated from tumor-bearing mice is related to reduce expression of the inducible nitric oxide synthase gene. J Exp Med **1996**;183:1323-9
41. Zhang T, Gong X, Hu G, Wang X. EP2-PKA signaling is suppressed by triptolide in lipopolysaccharide-induced microglia activation. J Neuroinflammation **2015**;12:50
42. Zelenay S, van der Veen AG, Bottcher JP, Snelgrove KJ, Rogers N, Acton SE, et al. Cyclooxygenase-Dependent Tumor Growth through Evasion of Immunity. Cell **2015**;162:1257-70
43. Kaplan DH, Shankaran V, Dighe AS, Stockert E, Aguet M, Old LJ, et al. Demonstration of an interferon gamma-dependent tumor surveillance system in immunocompetent mice. Proc Natl Acad Sci U S A **1998**;95:7556-61
44. Shankaran V, Ikeda H, Bruce AT, White JM, Swanson PE, Old LJ, et al. IFNgamma and lymphocytes prevent primary tumour development and shape tumour immunogenicity. Nature **2001**;410:1107-11
45. Wilke CM, Wei S, Wang L, Kryczek I, Kao J, Zou W. Dual biological effects of the cytokines interleukin-10 and interferon-gamma. Cancer Immunol Immunother **2011**;60:1529-41
46. Lawrence T, Natoli G. Transcriptional regulation of macrophage polarization: enabling diversity with identity. Nat Rev Immunol **2011**;11:750-61
47. Curiel TJ, Wei S, Dong H, Alvarez X, Cheng P, Mottram P, et al. Blockade of B7-H1 improves myeloid dendritic cell-mediated antitumor immunity. Nat Med **2003**;9:562-7

48. Wu K, Kryczek I, Chen L, Zou W, Welling TH. Kupffer cell suppression of CD8+ T cells in human hepatocellular carcinoma is mediated by B7-H1/programmed death-1 interactions. Cancer Res **2009**;69:8067-75
49. Platanias LC. Introduction: interferon signals: what is classical and what is nonclassical? J Interferon Cytokine Res **2005**;25:732
50. Ganster RW, Taylor BS, Shao L, Geller DA. Complex regulation of human inducible nitric oxide synthase gene transcription by Stat 1 and NF-kappa B. Proc Natl Acad Sci U S A **2001**;98:8638-43
51. Mao Y, Sarhan D, Steven A, Seliger B, Kiessling R, Lundqvist A. Inhibition of tumor-derived prostaglandin-e2 blocks the induction of myeloid-derived suppressor cells and recovers natural killer cell activity. Clin Cancer Res **2014**;20:4096-106
52. Kobayashi Y. The regulatory role of nitric oxide in proinflammatory cytokine expression during the induction and resolution of inflammation. J Leukoc Biol **2010**;88:1157-62
53. Ganesh T. Prostanoid receptor EP2 as a therapeutic target. J Med Chem **2014**;57:4454-65
54. O'Brien AJ, Fullerton JN, Massey KA, Auld G, Sewell G, James S, et al. Immunosuppression in acutely decompensated cirrhosis is mediated by prostaglandin E2. Nat Med **2014**;20:518-23
55. O'Callaghan G, Houston A. Prostaglandin E2 and the EP receptors in malignancy: possible therapeutic targets? Br J Pharmacol **2015**;172:5239-50

FIGURES LEGENDS

Figure 1. Role of p50 NF-κB in IFNγ-induced NO-dependent suppressive activity of M-MDSC. (A, left) Confocal microscopy showing selective up-regulation of nuclear p50 NF-κB in the splenic M-MDSC subset during tumor growth (day 21). (A, right) Quantification of p50 nuclear accumulation (***P<0.001 by two-tailed n=19 nuclei of M-MDSC day 11, n=18 nuclei of splenic M-MDSC day 21). (B) Inhibition of both tumor growth (MN/MCA1) (data shown are mean±SD *P<0.01 by two-tailed two-way ANOVA, n=9 WT and n= 8 $p50^{-/-}$ mice) and metastasis formation in p50 NF-κB–deficient mice (data shown are mean±SEM ***P<0.001 by two-tailed t-test, n=9 WT and n= 8 $p50^{-/-}$ mice). (C-D) Increased number of M-MDSC ($CD11b^{+}Ly6G^{-}Ly6C^{+}$ cells) in the spleen (C) and in the tumor (D) of $p50^{-/-}$ tumor-bearing mice (data

784 shown are mean±SEM *P<0.05 by two-tailed two-way ANOVA, n=5 WT and
785 n= 5 $p50^{-/-}$ mice). (E) Lack of p50 in M-MDSC impairs *Nos2* mRNA expression
786 in response to IFNγ (data shown are mean±SEM ***P<0.001, by two-tailed t-
787 test n=4 WT M-MDSC and n=4 $p50^{-/-}$ M-MDSC n=2 WT PMN-MDSC and n=2
788 $p50^{-/-}$ PMN-MDSC biological replicates each run in triplicate). (F) Reduced
789 IFNγ-mediated NO production in $p50^{-/-}$ M-MDSC (data shown are from a
790 representative experiment *P<0.05 by two-tailed t-test, n=3 WT and n=3 $p50^{-/-}$
791 technical replicates). (G-H) Both spleen (G) and tumor (H) $p50^{-/-}$ M-MDSC
792 showed a decreased ability to inhibit T cell proliferation in response to of IFNγ,
793 at different MDSC: splenocytes ratio (data shown are from a representative
794 experiment *P<0.05, ***P<0.001 by two-tailed t-test, n=3 WT and n=3 $p50^{-/-}$
795 technical replicates). (I) Left, decreased antigen-specific suppressive activity
796 of $p50^{-/-}$ M-MDSC in response to IFNγ, at different MDSC:OT1 splenocytes
797 ratio (data shown are from a representative experiment *P<0.05, ***P<0.001
798 by two-tailed t-test, n=3 WT and n=3 $p50^{-/-}$ technical replicates). Right,
799 decreased NO production in the co-culture supernatants of IFNγ-treated $p50^{-/-}$
800 M-MDSC, as compared to WT M-MDSC. L-NMMA, nitric oxide synthase
801 inhibitor. (data shown are from a representative experiment *P<0.05,
802 ***P<0.001 by two-tailed t-test, n=2 technical replicates). (J), Left, Increased
803 number of $CD33^{+}CD14^{+}HLA\text{-}DR^{low/-}$ cells in blood from CRC patients Right,
804 NOS2 expression from $CD14^{+}$ and $CD14^{+}HLA\text{-}DR^{low/-}CD33^{++}$ cells in blood
805 from healthy donors and CRC patients (*P<0.05 by two-tailed t-test n=3
806 healthy donors n=6 CRC patients). (K) Left, Representative confocal
807 microscopy on nuclear p50 in peripheral blood $CD14^{+}HLA\text{-}DR^{low/-}$ cells from
808 CRC patients, as compared to peripheral blood mononuclear $CD14^{+}$ cells

809 from healthy donors (scale bars are 10μm). Right, MFI of nuclear and nuclear
810 vs cytoplasmic ratio of p50 in $CD14^{+}HLA\text{-}DR^{low/-}$ cells from CRC patients
811 (**P<0.01; ***P<0.001 by two-tailed t-test, n=6 healthy donors n=9 CRC
812 patients).
813
814
815 **Figure 2. p50 deficiency in the BM stroma associates with enhanced**
816 **myelopoiesis**. BM cells from WT and $p50^{-/-}$ mice were stained with mAb to c-
817 Kit, Sca-1 and lineage- specific markers (CD3, CD11b, CD11c, Gr-1, B220,
818 ter119). LSK progenitors were defined as $Sca1^{+}$ cells within the gate of $lin^{-}c\text{-}Kit^{+}$
819 cells. (A) Representative FACS analysis of LSK progenitors in WT and
820 $p50^{-/-}$ BM. (B) Collective data showing that the fraction of LSK progenitors is
821 increased in $p50^{-/-}$ mice (*P<0.05 by two-tailed t-test n=6 WT and n=6 $p50^{-/-}$
822 mice). (C) Hematopoiesis was analyzed using a clonogenic colony culture
823 assay. The relative number of total BM-CFU, GM-CFU and M-CFU myeloid
824 colonies was significantly increased in $p50^{-/-}$ mice compared to the WT
825 counterpart. (**P<0.01 ***P<0.001 by two-tailed t-test n=6 WT and n=6 $p50^{-/-}$
826 mice). (D) Histopathological analysis (H&E) of the BM of p50-/- and control
827 WT mice. The BM hematopoietic parenchyma of p50-/- mice is characterized
828 by the marked impairment of terminal granulopoiesis and by the increase in
829 the density of immature myeloid precursors and blasts that show aggregation
830 in clusters. Red arrows indicate myeloid blasts. Original magnifications: upper
831 panels, scale bars are 100μm; lower panels, scale bars are 50μm. (E)
832 Monocytic differentiation is preserved in the BM of $p50^{-/-}$ mice, as testified by
833 the presence of cells with mature monocytic morphology and by the normal

density of hemosiderin-laden macrophages. scale bars are 50μm. (F) Fraction of mature Gr-1^{+}c-kit^{-} and immature Gr-1^{+}c-Kit^{+} granulocytes in BM from WT and p50$^{-/-}$ mice. The fraction of immature granulocytes is increased in the absence of p50 in comparison to the WT counterpart (***P<0.001 by two-tailed t-test n=6 WT and n=6 p50$^{-/-}$ mice). (G) Morphologic analysis (left) and quantification (right) of Giemsa-stained peripheral blood smears from 12 weeks-old p50$^{-/-}$ and WT mice showing that circulating granulocytes from p50$^{-/-}$ mice are enriched in immature and blast-like forms (*P<0.05 by two-tailed t-test n=6 WT and n=6 p50$^{-/-}$ mice). (**H**) Increased fraction of LSK progenitors in the BM of *p50$^{-/-}$* tumor bearing mice (*P<0.05 by two-tailed t-test n=5 WT and n=5 p50$^{-/-}$ mice). (**I**) Histopathological analysis (H&E) of the BM of tumor bearing mice showed a marked impairment of terminal granulopoiesis and an increased density of immature myeloid precursors and blasts in the BM hematopoietic parenchyma of p50$^{-/-}$ mice. Original magnifications: upper panels, scale bars are 100μm; lower panels, scale bars are 50μm. (J) Increased frequency of immature granulocytes (Gr1^{+}c-kit^{+} cells) in the BM of p50-/- tumor bearing mice (*P<0.05 by two-tailed t-test n=5 WT and n=5 p50$^{-/-}$ mice). (K) Cytofluorimetric analysis of IRF8 in M- (CD11b^{+}Ly6G^{-}Ly6C^{+} cells) and PMN-MDSC (CD11b^{+}Ly6G^{+}Ly6C$^{low/-}$ cells). (*P<0.05 by two-tailed t-test WT n=4, p50$^{-/-}$ n=6 mice).

Figure 3. Myeloid-specific p50 NF-κB reprograms innate ad adaptive immune functions (A) Splenic M-MDSC from p50$^{-/-}$ BM-transplanted mice display reduced suppressive activity (left) and NO production (right) in response to IFNγ. Proliferation was assessed by ^{3}H-thymidine incorporation

859 (*P<0.05; **P<0.01; ***P<0.001 by two-tailed one-way ANOVA n=6 technical
860 replicates of T cells only, n=3 technical replicates of pooled WT mice with WT
861 BM, n=3 technical replicates of pooled WT mice with $p50^{-/-}$ BM, n=3 technical
862 replicates of pooled $p50^{-/-}$ mice with WT BM, n=2 technical replicates of
863 pooled $p50^{-/-}$ mice with $p50^{-/-}$ BM). NO production by a technical triplicate
864 (n=3) for each group (***P<0.001 by two-tailed one-way ANOVA) (B) Left,
865 metastasis formation in control $p50^{flox}$ and $p50^{Tie2}$ mice (*P<0.05 by one-tailed
866 t-test; $p50^{flox}$ n=6; $p50^{Tie2}$ n=5). Center and right, increased number of splenic
867 and tumor infiltrating M-MDSC ($CD11b^{+}Ly6G^{-}Ly6C^{+}$) and PMN-MDSC
868 ($CD11b^{+}Ly6G^{+}Ly6C^{low/-}$) respectively in $p50^{Tie2}$ tumor-bearing mice (*P<0.05
869 by two-tailed t-test; spleen n=6 $p50^{flox}$ and n=6 $p50^{Tie2}$ tumor-bearing mice,
870 tumor n=4 $p50^{flox}$ and n=5 $p50^{Tie2}$ mice). (C) Top, flow cytometry analysis of
871 NOS2 in M-MDSC from both spleen (**P<0.01 by two-tailed t-test; n=4 $p50^{flox}$
872 and n=4 $p50^{Tie2}$ tumor-bearing mice) and tumor of $p50^{flox}$ and $p50^{Tie2}$ tumor-
873 bearing mice (**P<0.01 by two-tailed t-test; n=5 $p50^{flox}$ and n=5 $p50^{Tie2}$ mice).
874 Bottom, flow cytometry analysis of TNFα in tumor-infiltrating M- and PMN-
875 MDSC from $p50^{flox}$ and $p50^{Tie2}$ tumor-bearing mice (**P<0.01 by two-tailed t-
876 test; n=4 $p50^{flox}$ and n=3 $p50^{Tie2}$ mice). (D) Flow cytometry analysis of IFNγ
877 and GZMB-expressing $CD4^{+}$ and $CD8^{+}$ T cells in spleen and tumor from
878 $p50^{flox}$ and $p50^{Tie2}$ mice (*P<0.05, **P<0.01 by two-tailed t-test; spleen n=5
879 $p50^{flox}$ and n=4 $p50^{Tie2}$ tumor-bearing mice; IFNγ tumor n=6 $p50^{flox}$ and n=4
880 $p50^{Tie2}$ mice; GZMB tumor n=5 $p50^{flox}$ and n=5 $p50^{Tie2}$ mice). (E) Inhibition of
881 T cell proliferation by either spleen (left) or tumor (right) $p50^{Tie2}$ M-MDSC in
882 response to of IFNγ, at different MDSC: splenocytes ratio (data shown are

from a representative experiment *P<0.05, ***P<0.001 by two-tailed t-test, n=2 WT and n=2 $p50^{-/-}$ technical replicates).

Figure 4. **Effects of p50 deficiency on gene expression and STAT1 binding in splenic M-MDSC, from tumor bearing mice, treated with IFNγ**. (A) M-MDSC from WT and $p50^{-/-}$ tumor bearing mice were isolated from spleen and stimulated with IFNγ for 15'. Cells were stained with an anti-P-Stat1 antibody and analyzed by FACS (*P<0.05 by two-tailed t-test n=2 WT and n=2 $p50^{-/-}$ biological replicates) (B) Heatmap showing selective gene expression alterations in $p50^{-/-}$ M-MDSC stimulated with IFNγ for 4 hours (n=2 WT and n=2 $p50^{-/-}$ biological replicates). Data obtained with two biological replicates were highly correlated (R^2>0.97) indicating high reproducibility between samples. For each transcript, the expression level (log2-transformed FPKM) is z-score scaled (red: highly expressed; blue: lowly expressed). In the vertical bar, colors indicate six groups of genes (Red: IFNγ-induced genes up-regulated in $p50^{-/-}$ M-MDSC; orange: IFNγ–induced genes down-regulated in $p50^{-/-}$ M-MDSC; light grey: IFNγ–induced genes not affected by p50 ablation; blue: IFNγ–repressed genes down-regulated in p50-/- M-MDSC; light blue: IFNγ–repressed genes up-regulated in $p50^{-/-}$ M-MDSC; grey: IFNγ–repressed genes not affected by p50 ablation. The number of genes belonging to each group is indicated on the left. (C) A representative snapshot of RNAseq expression data for the *Nos2* and *Tnf* genes. (D) Chromatin immunoprecipitation showing impaired recruitment of STAT1 on regulatory

907 regions of the NOS2 promoter, in splenic M-MDSC from p50$^{-/-}$ tumor bearing
908 mice mice treated with IFNγ (P<0.001 by two-tailed one-way ANOVA n=3 WT
909 and n=3 p50$^{-/-}$ technical replicates).

910

911 **Figure 5. Ablation of p50 NF-κB in M-MDSC restores IFNγ-mediated**
912 **antitumor activity *in vivo***. (A) Left, antitumor effects of IFNγ in WT vs p50$^{-/-}$
913 mice. Center and right, *in vivo* depletion of CD4^{+} and CD8^{+} T cells in p50 NF-
914 κB-deficient tumor bearing mice abolishes the antitumor activity of IFNγ in
915 terms of tumor growth (data shown are mean±SEM P value was calculated by
916 two-tailed two-way ANOVA, n=5 WT vehicle treated mice, n=5 p50$^{-/-}$ vehicle
917 treated mice n=5 WT IFNγ treated mice, n=6 p50$^{-/-}$ IFNγ treated mice, n=6
918 p50$^{-/-}$ anti-CD4/CD8 and IFNγ treated mice) and metastasis formation
919 (***P<0.001 by two-tailed one-way ANOVA n=4 WT IFNγ treated mice, n=4
920 p50$^{-/-}$ IFNγ treated mice, n=5 p50$^{-/-}$ anti-CD4/CD8 and IFNγ treated mice). (B)
921 Adoptive transfer of WT M-MDSC in p50$^{-/-}$ tumor-bearing mice abolishes the
922 antitumor activity of IFNγ in vivo, restoring tumor growth. (data shown are
923 mean±SEM, P value was calculated by two-tailed two-way ANOVA n=8 WT
924 mice, n=8 p50$^{-/-}$ mice, n=7 p50$^{-/-}$ + WT M-MDSC mice, n=6 p50$^{-/-}$ + p50$^{-/-}$ M-
925 MDSC mice). (C-D) FACS analysis of CD4^{+} and CD8^{+} T cells for IFNγ and
926 GZMB expression and effector memory phenotype (CD62L^{-}CD44^{+}CD8^{+} T
927 cells) in both (C) spleen (*P<0.05, by two-tailed one-way ANOVA n=6 WT
928 mice, n=6 p50$^{-/-}$ mice, n=6 p50$^{-/-}$ + WT M-MDSC mice, n=5 p50$^{-/-}$ + p50$^{-/-}$ M-
929 MDSC mice) and (D) tumor (P<0.05, by two-tailed one-way ANOVA n=6 WT
930 mice, n=6 p50$^{-/-}$ mice, n=6 p50$^{-/-}$ + WT M-MDSC mice, n=6 p50$^{-/-}$ + p50$^{-/-}$ M-

MDSC mice) of tumor bearing mice. WT, WT mice; $p50^{-/-}$, $p50^{-/-}$ mice; $p50^{-/-}$ + WT M-MDSC, $p50^{-/-}$ mice adoptively transferred with WT M-MDSC; $p50^{-/-}$ + $p50^{-/-}$ M-MDSC, $p50^{-/-}$ mice adoptively transferred with $p50^{-/-}$ M-MDSC

Figure 6. Tumor-derived PGE2 promotes p50 NF-κB mediated suppressive M-MDSC functions. (A) Levels of IL-10, TGFβ, PGE2, GM-CSF, G-CSF and M-CSF in n=2 independent TSN, estimated by ELISA. (B) Right, confocal microscopy of p50 NF-κB in BM-derived M-MDSC conditioned with either TSN, PGE2 (10μM and 20 μM) or TSN plus the EP2 antagonist AH6809 or the EP4 antagonist AH23848 (scale bars are 10 μm). Post 48 hrs of in vitro activation, cells were stained with anti-p50 NF-κB antibody (green) and nuclei were counterstained with DAPI (blue). Left, confocal microscopy analysis of p50 NF-κB nuclear fluorescence intensity (**P<0.01, ***P<0.001, by two tailed one-way ANOVA, medium n=34 nuclei, PGE2 10 μM n=62 nuclei, PGE2 20 μM n=71 nuclei, TSN n=96 nuclei, TSN+AH6809 n=70 nuclei, TSN+AH23848 n=61 nuclei). (C) TSN primes IFNγ-treated MDSC for enhanced expression of *NOS2* mRNA and NO production (***P<0.001 by two-tailed one-way ANOVA, n=3 technical replicates of a representative experiment). (D) Inhibition of NO production by the EP2 receptor antagonist AH6809, in TSN-primed and IFNγ-treated WT and p50-deficient BM-MDSC. Both TSN and the selective EP2 agonist (butaprost) displayed priming activity for NO production in WT BM-MDSC, but not in the p50-deficient counterpart (**P<0.01, ***P<0.001 by two-tailed one-way ANOVA, n=3 technical replicates of a representative experiment). (E) Left, AH6809 inhibits fibrosarcoma growth

(data shown are mean±SEM *P<0.05 by two-tailed two-way ANOVA n=6 WT vehicle mice, n=6 WT AH6809 treated mice, n=6 $p50^{-/-}$ vehicle mice, n=6 $p50^{-/-}$ AH6809 treated mice) and lung metastasis formation in tumor bearing WT mice (**P<0.01 by two-tailed t-test n=5 WT vehicle treated mice, n=6 WT AH6809 treated mice). (F-G) FACS analysis of infiltrating immune cells in tumor (F) and spleen (G) of fibrosarcoma (MN/MCA1) bearing WT mice treated with AH6809 or untreated (vehicle). We evaluated expression of NOS2 and TNFα in M-MDSC and IFNγ in $CD4^+$ and $CD8^+$ T cells. Data pooled from two different experiments are shown (*P<0.05, **P<0.01 by two-tailed t-test. Tumor, TNFα in M-MDSC n=6 WT vehicle and n=6 WT AH6809 treated mice, NOS2 in M-MDSC n=7 WT vehicle and n=7 WT AH6809 treated mice; IFNγ in $CD4^+$ T cells n=6 WT vehicle and n=6 WT AH6809 treated mice; IFNγ in $CD8^+$ T cells n=7 WT vehicle and n=7 WT AH6809 treated mice. Spleen, NOS2 and TNFα in M-MDSC and IFNγ in $CD8^+$ T cells n=4 WT vehicle and n=4 WT AH6809 treated mice, IFNγ in $CD4^+$ T cells n=3 WT vehicle and n=3 WT AH6809 treated mice).

Figure 7: Blocking NO production restores the anti-tumor activity of IFNγ in vivo. (A) L-NMMA treatment reduces melanoma (B16) growth in WT mice and releases the antitumor activity of IFNγ (data shown are mean±SEM P value was calculated by two-tailed two-way ANOVA n=5 WT Vehicle treated mice, n=5 IFNγ treated mice, n=5 L-NMMA treated mice, n=5 IFNγ + L-NMMA treated mice). (B) L-NMMA reduces the expression of NOS2 (Top) and increases the expression of TNFα (Bottom), in tumor-infiltrating M-MDSC (*P<0.05 by two-tailed one-way ANOVA n=5 WT Vehicle treated mice, n=5

IFNγ treated mice, n=5 L-NMMA treated mice, n=5 IFNγ+L-NMMA treated mice). (C) L-NMMA enhances tumor infiltration of IFNγ-expressing $CD8^+$ T cells (*P<0.05 by two-tailed one-way ANOVA n=4 WT Vehicle treated mice, n=5 IFNγ treated mice, n=5 L-NMMA treated mice, n=4 IFNγ+L-NMMA treated mice). (D) Representative flow cytometry of EP2 receptor and NOS2 expression in peripheral blood M-MDSC from CRC patients (n=5 CRC patients). (E) Flow cytometry analysis of NOS2 in IFNγ-treated human peripheral blood monocytes primed with TSN from the human pancreatic carcinoma cell line PANC1, in the presence or absence of the EP2 antagonist AH6809.

Figure 1

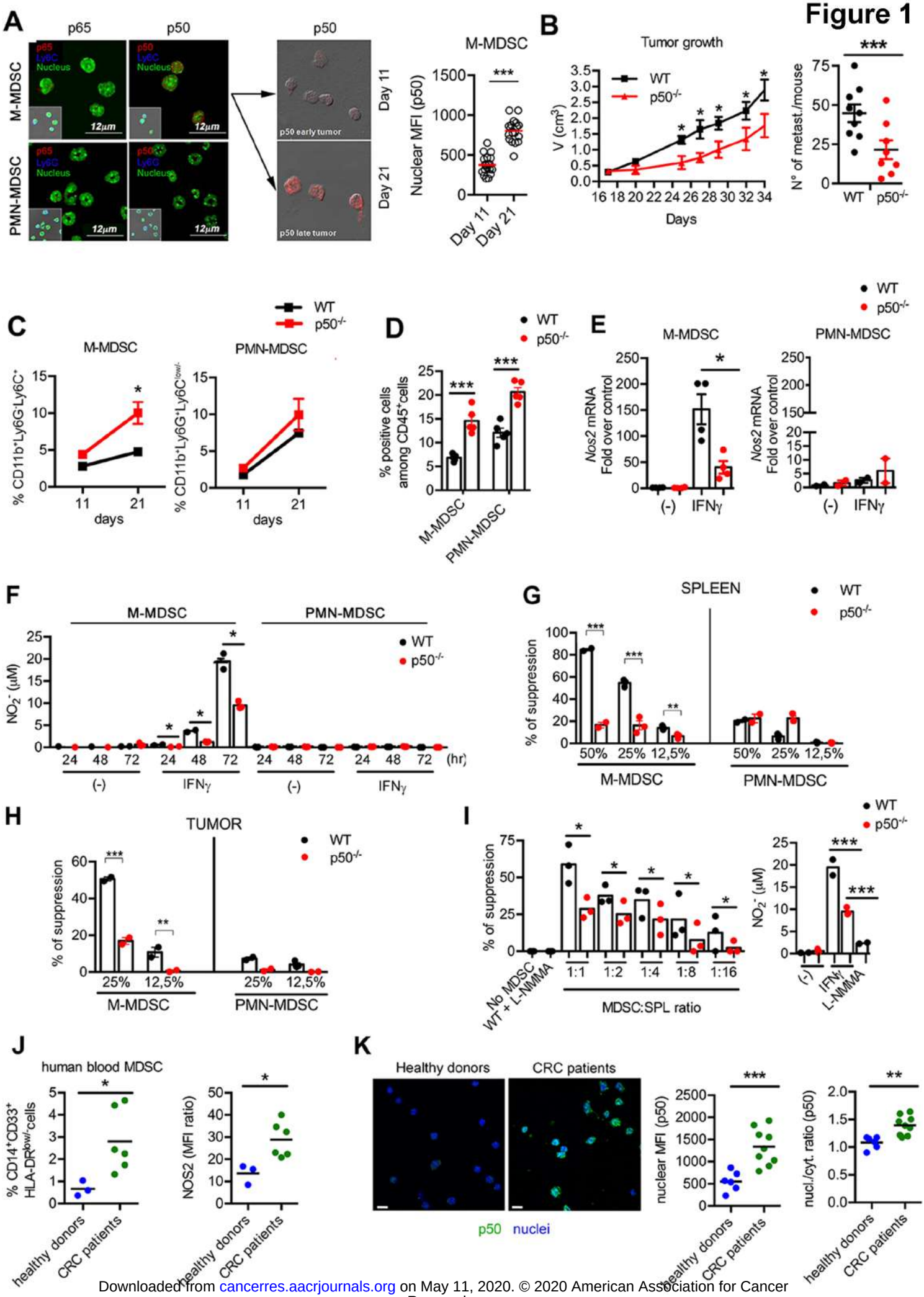

Figure 2

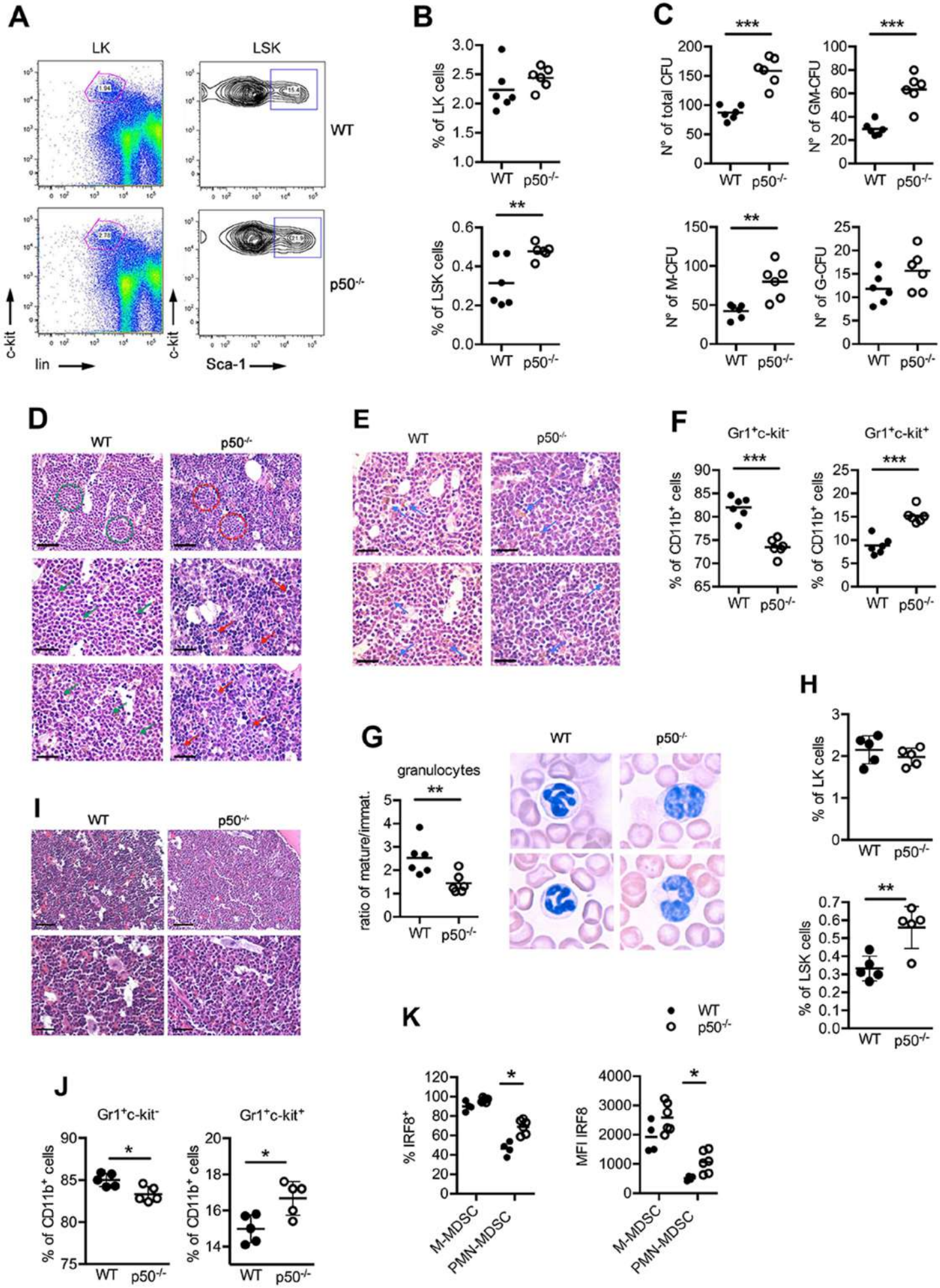

Figure 3

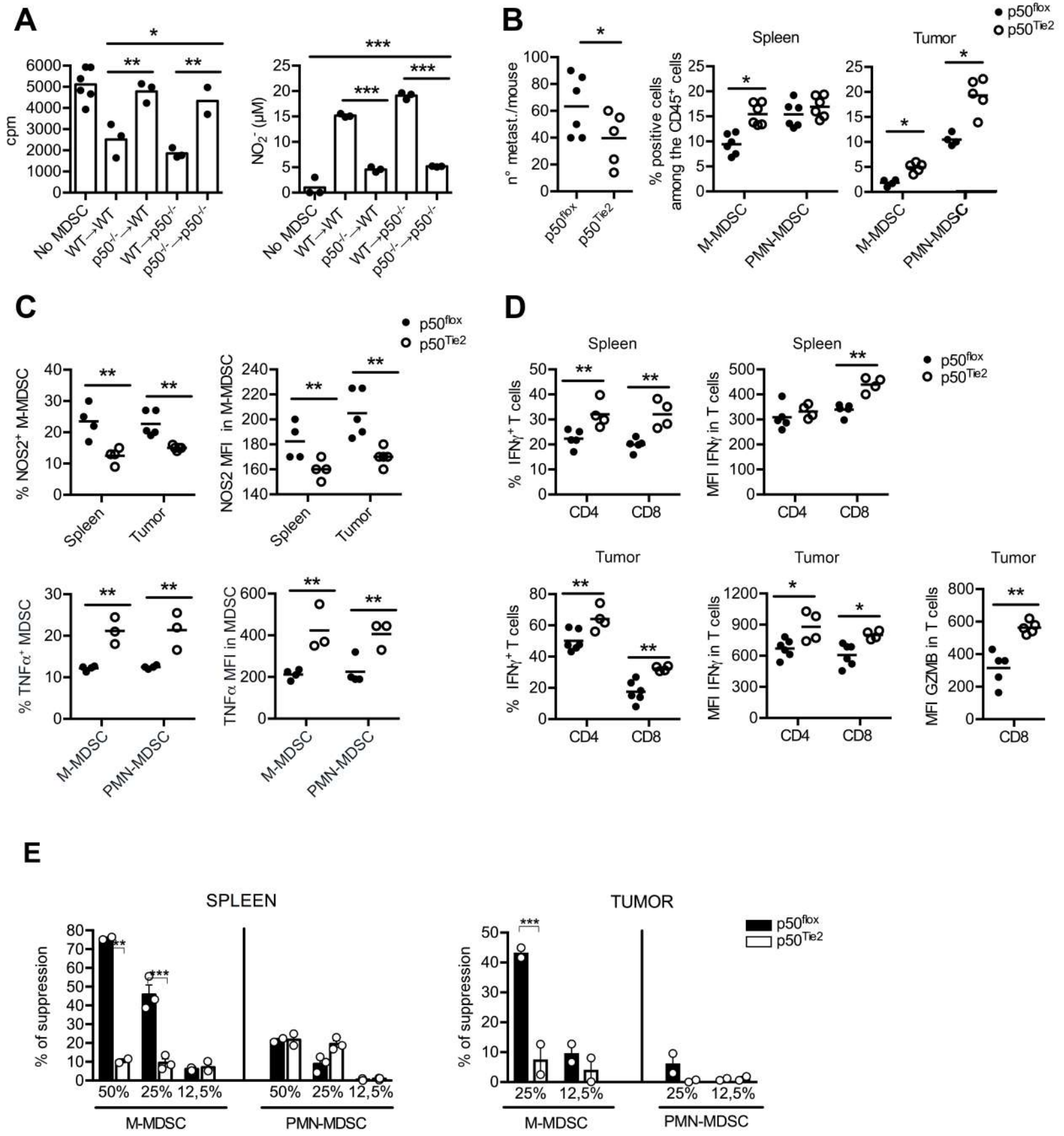

Figure 4

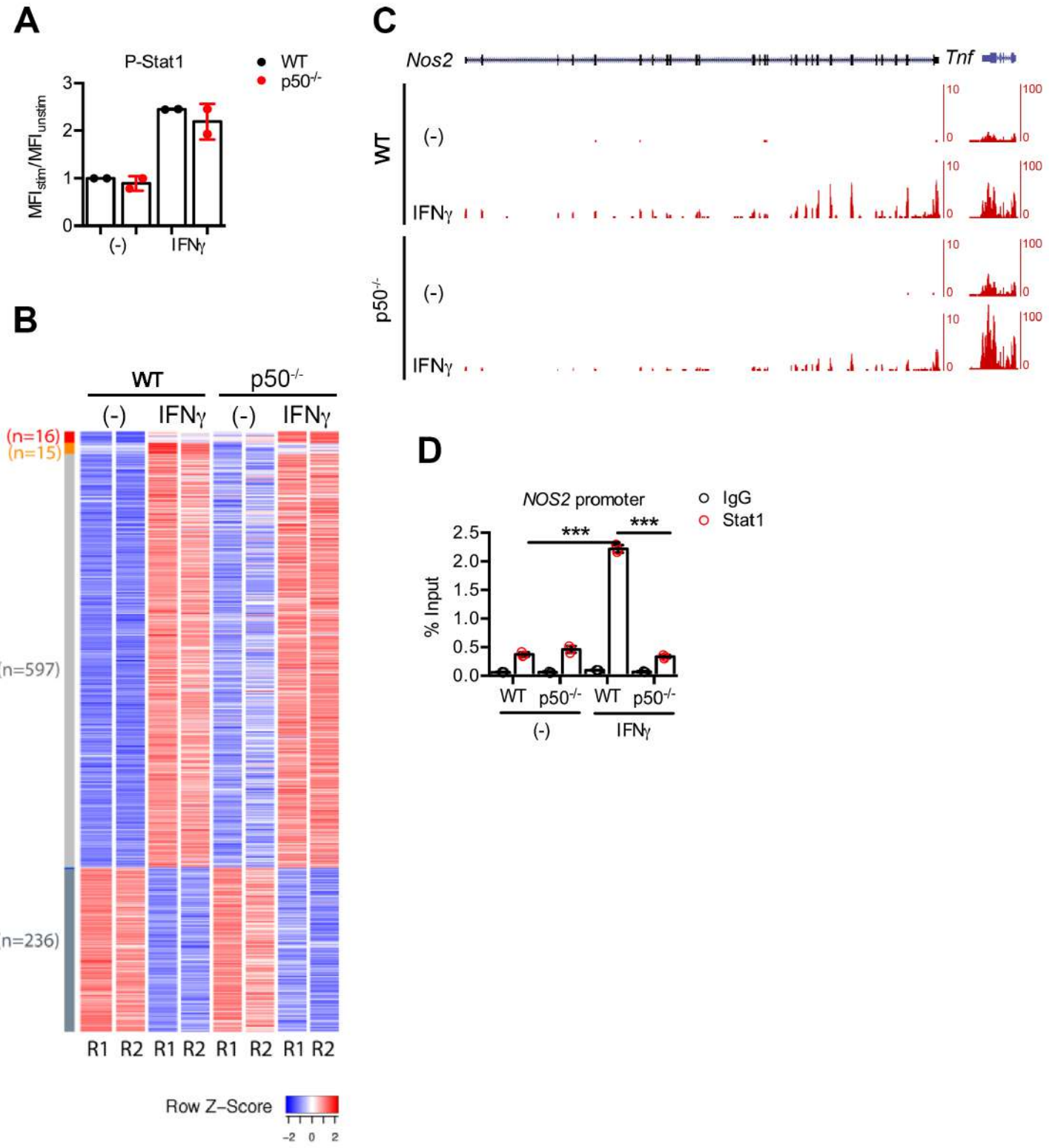

Figure 5

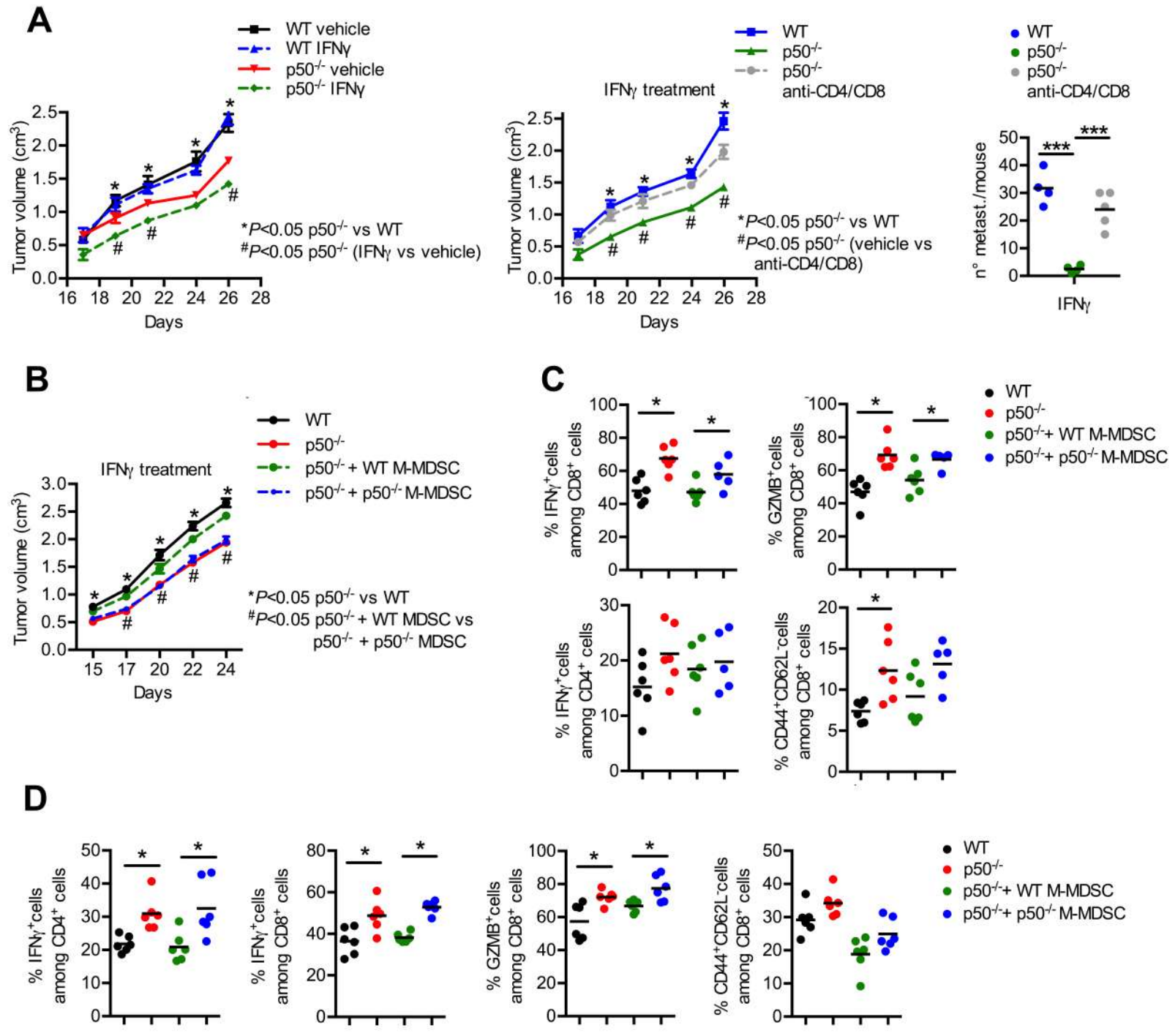

Figure 6

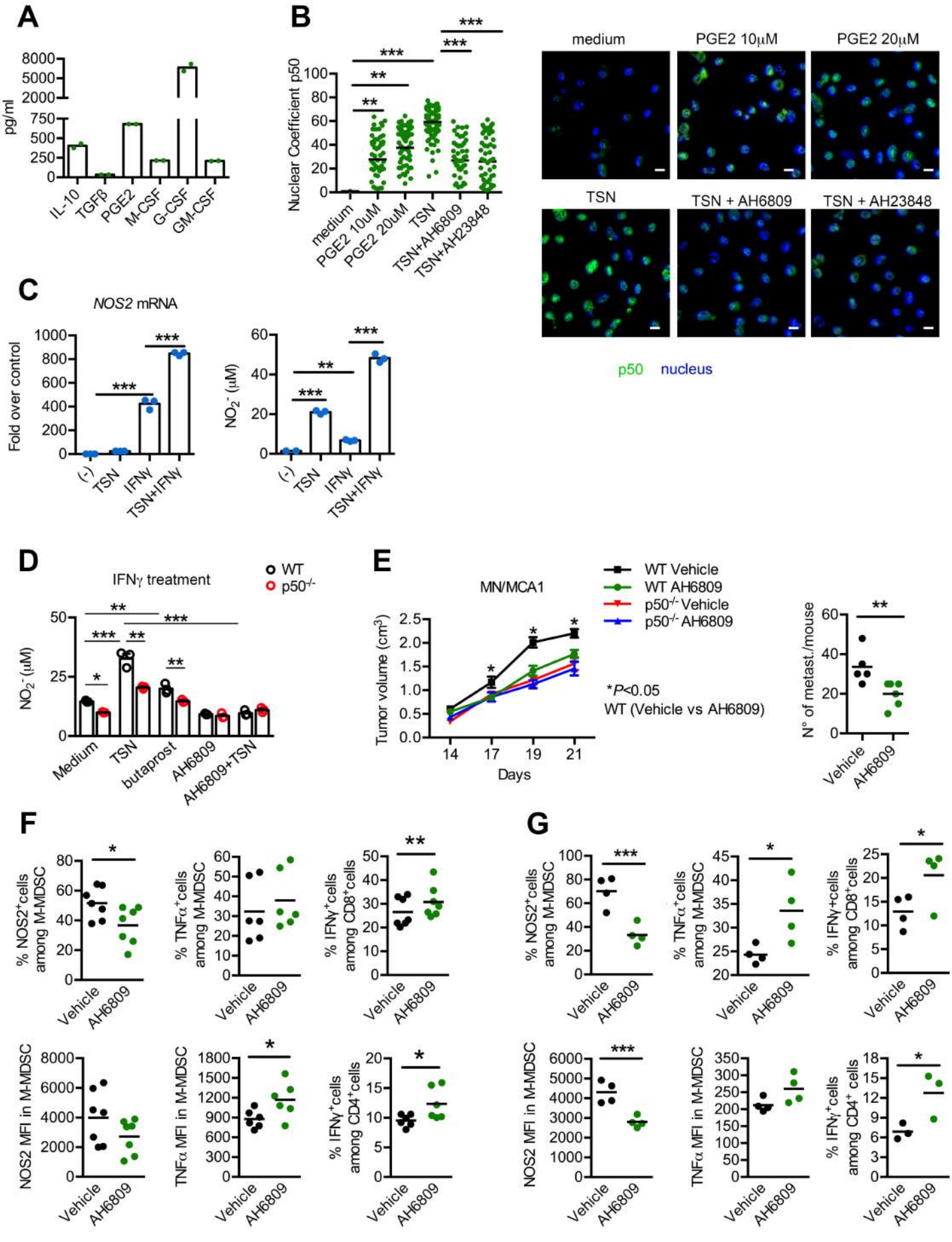

Figure 7

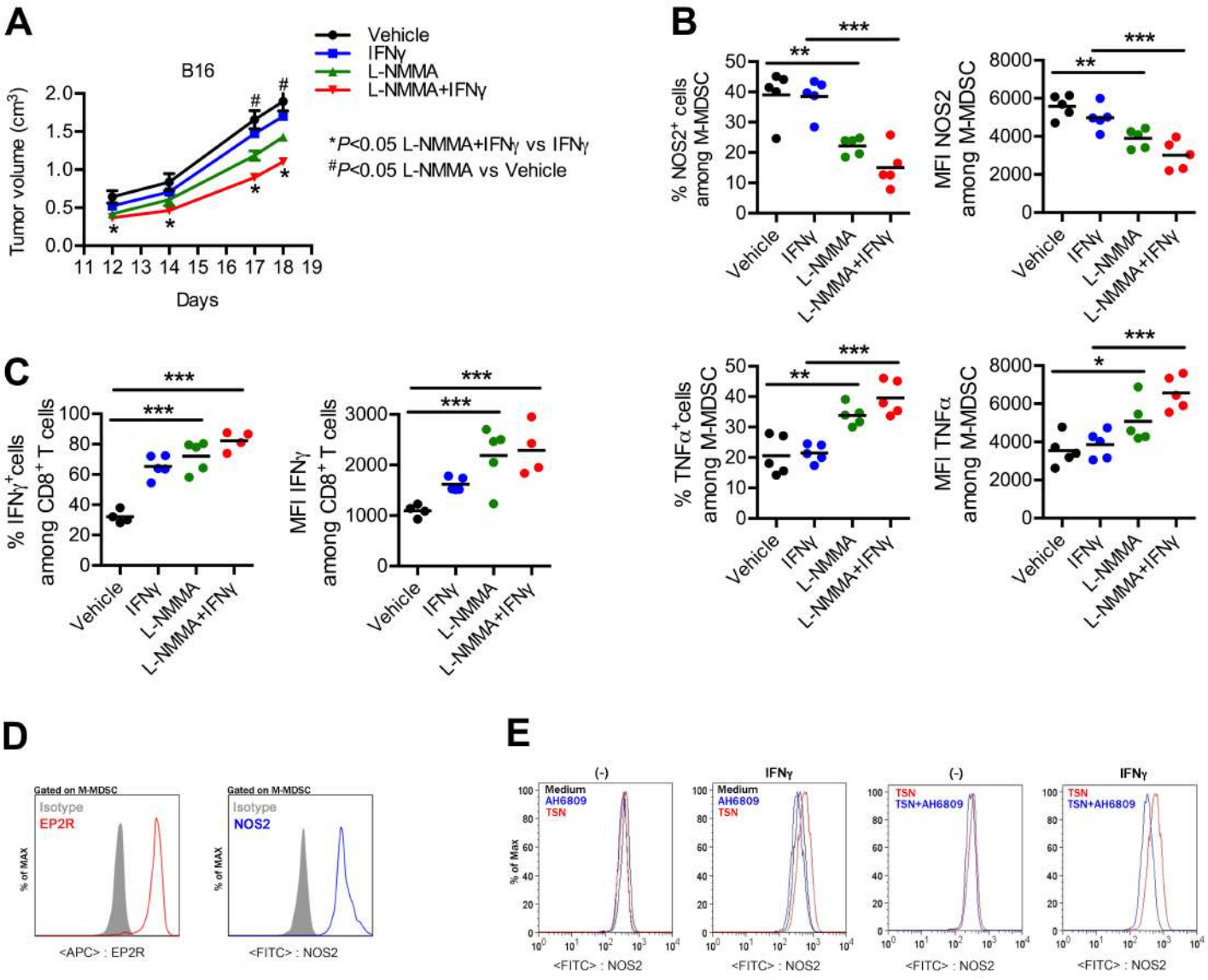

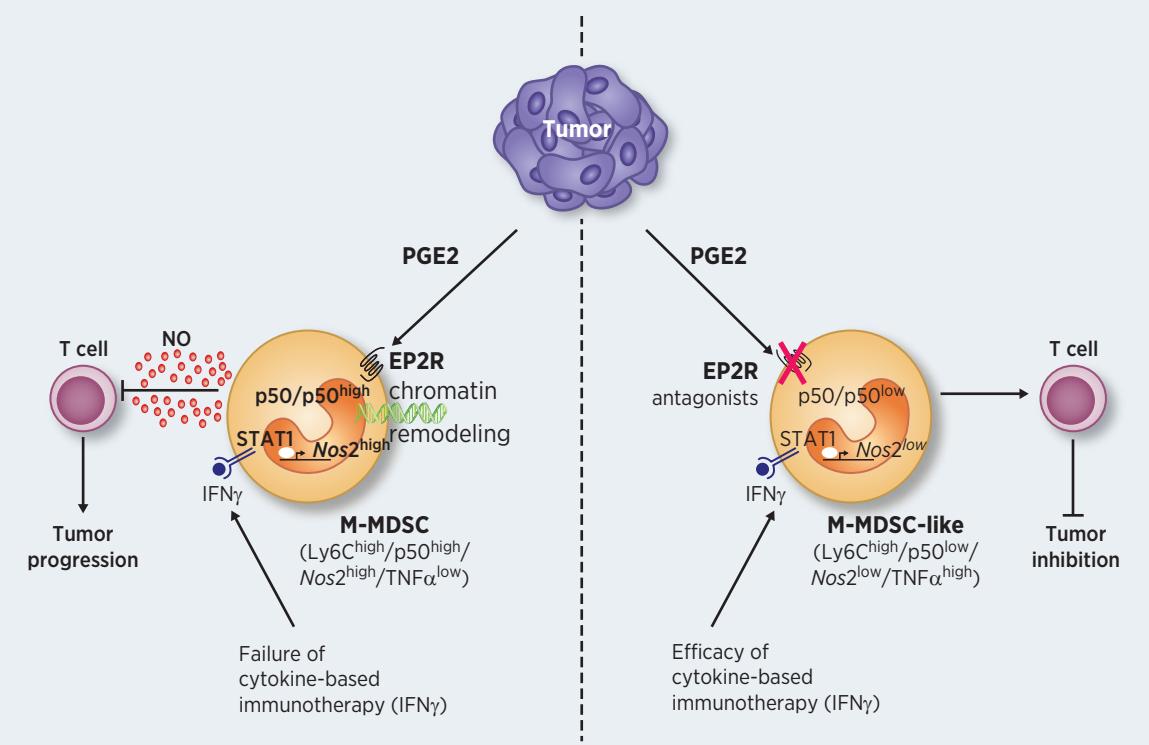

Tumor-derived PGE2-mediated induction of nuclear p50 NF-κB epigenetically reprograms the response of M-MDSC to IFNγ towards a NO-mediated immunosuppressive and tumor promoting phenotype.

AACR American Association for Cancer Research

Cancer Research

The Journal of Cancer Research (1916–1930) | The American Journal of Cancer (1931–1940)

Tumor-derived prostaglandin E2 promotes p50 NF-κB-dependent differentiation of monocytic MDSC

Chiara Porta, Francesca Maria Consonni, Sara Morlacchi, et al.

Cancer Res Published OnlineFirst April 7, 2020.